Mon. Not. R. astr. Soc. (1989) **239**, 571–603

The mass distribution in the galactic disc – I. A technique to determine the integral surface mass density of the disc near the Sun

Konrad Kuijken and Gerard Gilmore *Institute of Astronomy, Madingley Road, Cambridge CB3 0HA*

Accepted 1989 February 3. Received 1989 February 3; in original form 1988 November 1

Summary. We present a new technique for the determination of the integral surface mass density of the galactic disc at the solar galactocentric distance. The requisite observational data are an observed distribution function of velocities and distances for a sample of tracer stars extending $\gtrsim 1$ kpc from the galactic plane, and the spatial density distribution corresponding to that tracer population. The analysis involves comparison of the observed distribution function with a variety of model distribution functions, calculated for a wide range of assumed galactic potentials and corresponding force laws $K_z(z)$, to determine the best description of the data. The model distributions are calculated in a sufficiently general way that one can include the quite large effects due to the likely change in the orientation of the stellar velocity ellipsoid as one moves further from the galactic plane. The derived best fit K_z-force law is constrained to be consistent dynamically, in that the local mass density of the extended dark halo generating a large part of the radial acceleration in the Galaxy is also determined, in such a way as to ensure consistency with the observed rotation curve. An important feature of the analysis technique is that it utilizes the full observed distribution function, and so avoids the need for binning data and the use of a few velocity moments to represent a large number of observations.

1 Introduction

There are two related yet different measures of the distribution of mass in the galactic disc near the Sun. The most widely used and commonly determined measure is the local *volume* mass density – i.e. the amount of mass per unit volume near the Sun, which for practical purposes is the same as the volume mass density at the galactic plane. This quantity has units of $M_\odot$ pc^{-3}, and its local value is often called the 'Oort limit'. The contribution of the identified material to the Oort limit may be determined by summing all local observed matter – an observationally difficult task, which leads to considerable uncertainties. The uncertainties arise in part due to

difficulties in detecting very low luminosity stars, even very near the Sun (*cf.* Gilmore, Reid & Hewett 1985), but mostly from uncertainties in the appropriate volume density of the interstellar medium (ISM) to adopt. This latter uncertainty is exacerbated since the physically important quantity (for dynamical purposes) is the mean volume density of the patchily distributed ISM at the solar galactocentric distance. The dynamical determination of the Oort limit has an extensive history, and will be discussed further in Paper III of this series (Kuijken & Gilmore 1989b).

The second measure of the distribution of mass in the solar vicinity is the integral surface mass density. This quantity has units of $M_\odot$ pc^{-2}, and is the amount of disc mass in a column perpendicular to the galactic plane, extending sufficiently far that it includes all the mass associated with the galactic disc. It is this quantity which is of relevance to the interpretation of rotation curves and the large-scale distribution of mass in galaxies.

Both these quantities are derived from a measurement of the vertical galactic force field, $K_z(z)$, at the solar galactocentric distance $R = R_0$.

If one knew both the local *volume* mass density and the integral *surface* mass density of the galactic disc, one could immediately determine (or at least constrain) the scaleheight of any contribution to the local volume mass density which was not identified, even without knowing its nature. For example, one might deduce that some fraction of the local volume mass density was unidentified (i.e. a local 'missing mass' problem), but also determine a surface density which is effectively fully explained by observed mass. Then the unidentified contribution to the local volume density would have to have a small scaleheight, in order that its contribution to the surface density be small. It would then be plausible to deduce that any 'local' missing mass unidentified in the volume mass density near the Sun was not the same 'missing mass' which dominates the extended outer parts of galaxies.

Determination of the volume mass density and the integral surface mass density near the Sun require similar observational data, namely distances and velocities for a sample of suitable tracer stars (though on more distant tracers in the latter case), but rather different analyses. There are several inherent limitations in published techniques for a study of kinematic data, which, while not being a problem for determination of local dynamical quantities such as the Oort limit, are a major limitation in determination of more general dynamical quantities such as the integral surface density. In this paper we present a new technique for the analysis of stellar kinematic data, which is also appropriate for determination of the integral surface mass density of the galactic disc near the Sun. It involves maximum likelihood comparison of observed and predicted distribution functions of stellar velociites as a function of distance from the plane. It thus removes the need to describe an array of distance-velocity data by moments, such as the r.m.s. velocity dispersion. It also provides the freedom to include important physical effects (the orientation of the stellar velocity ellipsoid far from the galactic plane) and constraints (consistency with the galactic rotation curve) in the modelling.

In Paper II of this series (Kuijken & Gilmore 1989a) we apply this technique to a new data-set, and determine the integral surface mass density of the galactic disc. In Paper III (Kuijken & Gilmore 1989b) we readdress the determination of the local volume mass density – the Oort limit – near the Sun, and discuss the consistency of these local and more global dynamical quantities.

2 The measurement of galactic potentials

How can we measure the gravitational field in a stellar system? The obvious thing to do would be to launch a test-particle, and watch its orbit. Then we could calculate the force it feels at any point along its trajectory, and, after a few revolutions and vertical oscillations, deduce the

gravitational potential near this orbit. While such a procedure is feasible for studying the gravitational field of the Earth (after account is taken of atmospheric drag and other non-gravitational effects), as well as for study of the solar system and of some binary stars, for systems more than a few AU across the time-scales involved make investigations of this type impractical. We must therefore turn to the theory of stellar statistics, and use the ensemble of stellar positions and velocities measurable at a single time to study the gravitational potential. Excellent reviews of this subject can be found in Oort (1965), and in Binney & Tremaine (1987).

2.1 THE COLLISIONLESS BOLTZMANN EQUATION

The dynamics of any large stellar system are governed by the collisionless Boltzmann equation

$$\frac{Df}{Dt}\equiv\frac{\partial f}{\partial t}+\frac{\partial\vec{x}}{\partial t}\cdot\frac{\partial f}{\partial\vec{x}}+\frac{\partial\vec{v}}{\partial t}\cdot\frac{\partial f}{\partial\vec{v}}=0, \tag{1}$$

where f is the phase space density at the point $(\vec{x},\vec{v})$ in phase space [i.e. there are $f(\vec{x},\vec{v})\,d^3\vec{x}d^3\vec{v}$ stars in a volume of size $d^3\vec{x}$ centred on $\vec{x}$ with velocity in the volume of size $d^3\vec{v}$ about $\vec{v}$]. Such a distribution function is called 'fine-grained', as its construction requires averaging over infinitely small volumes. Sometimes, the structure of the orbit is so complicated (fractal) that is not possible to define such an $f(\vec{x},\vec{v})$, but for the moment we will ignore such complications, as is appropriate for systems comprised predominantly of regular orbits. A discussion of the occurrence of irregular orbits in the Milky Way Galaxy will be deferred until Appendix B.

The collisionless Boltzmann equation is satisfied by *any* stellar population, whether other stars are present or not. This arises because stars do not interact except through long-range gravity forces, and those are being described through a smooth background potential. Consequently, f does not have to describe the entire Galaxy; one can concentrate on any subsample of stars, and apply the collisionless Boltzmann equation to it. We will refer to such subsamples as *tracer populations*, since we may use their kinematics to trace the potential of the Galaxy, irrespective of what causes this potential.

If we have a steady-state tracer population, and a time-independent potential, as the large-scale field in the Milky Way presumably is, we can set

$$\frac{\partial f}{\partial t}=0. \tag{2}$$

For present purposes, the Galaxy is adequately described as being rotationally symmetric, so that it is convenient to write out the collisionless Boltzmann equation in cylindrical polar coordinates (R,ϕ,z) in which $z=0$ is the disc plane of symmetry, with corresponding velocity components (v_R,v_ϕ,v_z):

$$v_R\frac{\partial f}{\partial R}+v_z\frac{\partial f}{\partial z}+\left(K_R+\frac{v_\phi^2}{R}\right)\frac{\partial f}{\partial v_R}-\frac{v_Rv_\phi}{R}\frac{\partial f}{\partial v_\phi}+K_z\frac{\partial f}{\partial v_z}=0, \tag{3}$$

where the accelerations $\dot{v}_R$, $\dot{v}_\phi$, $\dot{v}_z$ explicit in equation (1) have been equated to the forces (real and fictitious) that cause them, and ϕ-gradients in f and in the potential set to zero. The vector $\vec{K}(R,z)$ is the gravity force. Then clearly knowledge of $f(\vec{x},\vec{v})$ allows the force components K_R and K_z to be derived. Note, though, that a general function f will not allow a solution for K_R and K_z: f has five independent variables (we suppressed any ϕ-dependence) and so cannot in general be made to satisfy an equation such as (3) which contains only two functions of two

variables. Since equation (3) cannot easily be solved in general with real data, one simplifies the analysis and proceeds by taking velocity moments. Multiplying through by v_z and by v_R and integrating over all velocity space produces Jeans' equations:

$$\nu K_z = \frac{\partial}{\partial z}(\nu\sigma_{zz}^2) + \frac{1}{R}\frac{\partial}{\partial R}(R\nu\sigma_{Rz}^2) \tag{4}$$

$$\nu K_R = \frac{1}{R}\frac{\partial}{\partial R}(R\nu\sigma_{RR}^2) + \frac{\partial}{\partial z}(\nu\sigma_{Rz}^2) - \frac{\nu\sigma_{\phi\phi}^2}{R}, \tag{5}$$

where $\nu(R,z)$ is the space density of the stars, and $\vec{\sigma}(R,z)$ their velocity dispersion tensor (i.e. $\sigma_{ij}^2 = \langle v_i v_j \rangle$). In this way we have separated the two force components, and can in principle derive them both from measurements of the moments of the velocity distributions and density of a stellar tracer population. We will mainly be interested in the K_z-equation (4), and will refer to it as 'the' Jeans' equation in future.

3 Application to disc galaxies

For a disc galaxy, the dominant gradient in the Jeans' equation is the z-gradient, provided we stay reasonably close to the plane. Therefore, we will for the present ignore the σ_{Rz} term, and return to its treatment later on (see Section 7 below). Most stellar orbits in the disc populations have quite low eccentricity, so that they confine themselves to a small range of R. Therefore, the z-force $K_z(R,z)$ changes little with R during an orbit, and the R- and z-motions are virtually independent. This means that it is possible to have as a solution of the collisionless Boltzmann equation a distribution function which separates into two factors, $f(R,v_R,v_\phi,z,v_z) = f_{R,\phi}(R,v_R,v_\phi) \times f_z(z,v_z)$. In this case the collisionless Boltzmann equation (3) separates as well, giving us the z-terms

$$v_z \frac{\partial f_z}{\partial z} + K_z \frac{\partial f_z}{\partial v_z} = 0 \tag{6}$$

with as solution

$$f_z(z,v_z) = f_z(E_z), \tag{7}$$

where $E_z = \psi(z) + \frac{1}{2}v_z^2$ and $d\psi(z)/dz = -K_z$. In other words, the energy E_z is the only integral of motion in this idealized one-dimensional stellar system.

So how can we obtain K_z in the case of a distribution function which obeys equation (7)? We require two observables pertaining to a suitable tracer population: the density $\nu(z)$, which can be derived from star counts, and the v_z-distribution as a function of z, $f_v(v_z;z)$. We somehow have to extract the potential $\psi(z)$ from these; there are many ways of doing this.

3.1 DIRECT CONTOURING OF $f_z(z,v_z)$

The most direct method of recovering $\psi(z)$ is probably by finding the curves of constant f_z in the (z,v_z) phase space. By equation (7), these are curves of constant $E_z = \psi(z) + \frac{1}{2}v_z^2$, from which $\psi(z)$ can be derived. Note that a function $f_z(z,v_z)$ in general will not admit a solution for $\psi(z)$ for which this is true; $f_z(z,v_z)$ only has two one-variable functional degrees of freedom, not as much as a general function of two variables. This becomes clear if we plot the contours of f_z in

the (z, v_z^2)-plane: in these coordinates, all the contours must have the same shape, since they all have to satisfy

$$\tfrac{1}{2}v_z^2 = E_z - \psi(z), \tag{8}$$

being curves of constant energy (see Fig. 1). Since we are dealing with real data rather than completely well-known functions, we have to try in some way to find the f_z that satisfies these constraints and is most consistent with the data.

If we try to measure $\psi(z)$ from the contours of f_z for a real dataset, we run into several potential problems:

(i) The data have to be binned in some way, as we are dealing with only a finite number of data points. For the number of velocity observations that is typically available (*cf.* paper II), the bins needed to obtain reasonable statistics have to be large. Since the quantity we are interested in is the derivative of the potential, coarse bins make it hard to obtain a good derivative.

(ii) Measurement errors in the velocities are difficult to deal with. They will mainly affect the velocity distribution where it is steepest, i.e. near $v_z = \langle |v_z| \rangle$; but this is where most of the stars are. A lot of weight ends up being put on the poorly defined wings of the distribution.

(iii) Not all the stars from which density laws are calculated have their radial velocity measured, and moreover the fraction of the stars which do have velocities may depend on the distance. This distance bias has to be taken into account.

(iv) The error analysis is complicated.

Making reliable deductions from direct contouring of a dataset containing only a few hundred stars is clearly not feasible. However, in Section 3.4 we will develop this idea further to take account of the physical constraints on the potential, of observational errors and of the uneven sampling of the stars with radial velocity data. A fit to the entire distribution function, which makes full use of the dataset, forms the underlying idea behind our method of analysis.

3.2 MOMENT EQUATIONS

We can of course use the velocity moments of equation (6) instead, analogous to the Jeans' equation (4). The zeroeth, first and second moments are (integrating over the range 0 to ∞ so

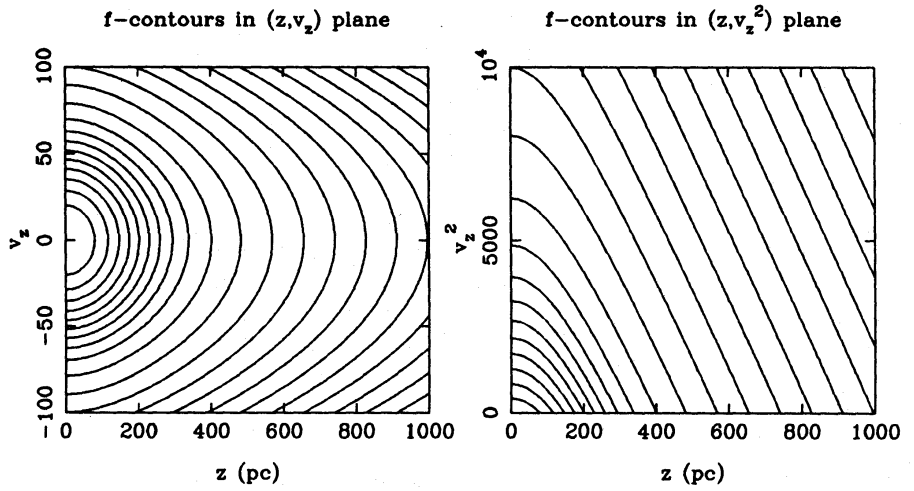

Figure 1. Contours of constant phase-space density in the distance-velocity (z, v_z)- and the (z, v_z^2)-planes. The shape of the contours yields the potential $\psi(z)$, and their separation yields the distribution function, $f_z(E_z)$.

that we can use odd velocity moments of the velocity distribution too)

$$f_z(z,0)\,K_z = \frac{1}{2}\frac{\partial}{\partial z}(\nu\langle|v_z|\rangle) \tag{9}$$

$$\nu K_z = \frac{\partial}{\partial z}(\nu\langle v_z^2\rangle) \tag{10}$$

$$(\nu\langle|v_z|\rangle)\,K_z = \frac{1}{2}\frac{\partial}{\partial z}(\nu\langle|v_z|^3\rangle); \tag{11}$$

the general term in this series is (for $n>0$)

$$(\nu\langle|v_z|^{n-1}\rangle)\,K_z = \frac{1}{n}\frac{\partial}{\partial z}(\nu\langle|v_z|^{n+1}\rangle). \tag{12}$$

(The terms on the left are obtained by integrating by parts the terms involving $\partial f_z/\partial v_z$.) Equation (10) is just the Jeans' equation back again, but without the σ_{Rz}-term, which vanishes for distribution functions which separate in cylindrical polar coordinates. This equation is the simplest to work with in this series, only requiring the density and the rms v_z-dispersions at various z's; however, this simplicity hides several drawbacks:

(i) By using only the second moment of the data, we throw away a lot of the available information about the velocity distribution. In fact, a run of density and velocity dispersion with z uniquely specifies the entire distribution function f_z, of which the second moment is only one aspect. We could instead have used any of the other moment equations (12) – in general this will not yield the same potential, because of inaccuracies in the measurements. We should really compare the data with the velocity distribution function itself, rather than restrict ourselves to a particular moment of it, as then all the constraints between the various moments are automatically satisfied. In any case, f_z should be calculated, to verify the fundamental physical requirement that it is everywhere non-negative: it is quite possible that a particular fit to the velocity dispersion profile implies a non-positive f_z, while nevertheless some other acceptable fit with a sensible underlying distribution function might well exist.

(ii) Unless large numbers of stars are available, $\langle v_z^2\rangle$ is not a very reliable statistic, in that it can be very sensitive to a few high-velocity stars in the data. To get around this problem, what has often been done is to convert the more stable statistic $\langle|v_z|\rangle$ into an *estimated* rms velocity dispersion, by assuming the shape of the velocity distribution to be Gaussian. This is mathematically incorrect, but nevertheless a useful approximation: for example, if we have equal numbers of stars in two populations, one of twice the dispersion of the other, then the ratio $\langle v_z^2\rangle/\langle|v_z|\rangle^2$ takes a value $\frac{10}{9}$ as high as for a Gaussian. This agreement is reasonably good, but if populations of higher velocity dispersion ratios are present, this rapidly becomes a worse approximation.

King (1965) has generalized the formalism of velocity moments to negative powers, which he calls 'pseudo-moments'. The '-2'-moment is particularly useful, since the analogue of equation (12) then does not contain a gradient in velocity dispersion, only one in density. These moments cannot be evaluated directly from velocity distribution data, however; one has to fit an appropriate analytic function to the data first, before being able to obtain this pseudo-moment. Therefore, unless the observed velocity distribution is very well-defined, an *a priori* idea of the shape of the velocity distribution is necessary. If this is known, one may use the techniques of this paper to fit that distribution directly.

Use of moment equations to derive the potential gradient relies strictly on local measurements of density and dispersion and their gradients, while, as we will see, the relation between the space density and the phase space density of a stellar population is far from local. Unless we have a single isothermal population, this method can give misleading results.

3.3 ISOTHERMAL COMPONENTS OF $f_z(E_z)$

A commonly used method is to model the distribution function of the tracer stars as one or more *isothermal* components. An isothermal component by definition has constant velocity dispersion, independent of z. Then one can easily see that the velocity distribution has to be Gaussian: by equation (10), if σ_{zz} is independent of z,

$$\nu(z) \propto \mathrm{e}^{-\psi(z)/\sigma_{zz}^2}, \tag{13}$$

and hence the Abel inversion described below (equation 21) yields

$$f_z(E_z) \propto \mathrm{e}^{-E_z/\sigma_{zz}^2} \propto \mathrm{e}^{-1/2(v_z^2/\sigma_{zz}^2)}. \tag{14}$$

This method is especially useful if the tracer appears to be a single isothermal component, as then the Jeans' equation simplifies to

$$K_z = \sigma_{zz}^2 \frac{\partial}{\partial z}[\ln \nu(z)] \tag{15}$$

and only the density gradient of the tracer population is needed.

Deconvolving non-isothermal populations into isothermal components is not easy, though. First, there is the question of how physically meaningful it really is to separate a stellar sample into discrete isothermal subsamples. Given continual star formation and the continuous diffusion processes thought to be active in heating the disc, this can at best be only an *ad hoc* approximation to the true distribution. A very large number of discrete isothermals is clearly necessary for a close approximation to a real galactic disc. Second, as we shall see, such deconvolutions are far from unique, leading to non-unique force laws.

At distance z_j, a superposition of N_{iso} isothermal components, each with velocity dispersion $\sigma_{zz,i}^2$ and density ν_i at $z=0$ has density

$$\nu(z_j) = \sum_{i=1}^{N_{\mathrm{iso}}} \nu_i \mathrm{e}^{-\psi(z_j)/\sigma_{zz,i}^2}. \tag{16}$$

This shows that at different distances from the plane the relative densities of the components are not the same, but that those of highest velocity dispersion dominate increasingly at higher z. If we were able to specify the $\sigma_{zz,i}$ and the ν_i of all components, this would allow a direct solution for the potential from the density profile. However, in practice we have to derive the ν_i of the high-velocity dispersion components from high-z velocity data, as at greater heights these components are more in evidence. But for $z \neq 0$, the relative densities of the isothermal components depend on the potential as well as the ν_i: thus we are faced with a self-consistency problem if we wish to solve for the potential.

At height z_j, the mth velocity moment of our superposition of isothermals is

$$\langle |v_z|^m \rangle (z_j) = \frac{\Sigma_i \nu_i \mathrm{e}^{-\psi(z_j)/\sigma_{zz,i}^2} (2\sigma_{zz,i}^2/\pi)^{m/2} [(m-1)/2]!}{\Sigma_i \nu_i \mathrm{e}^{-\psi(z_j)/\sigma_{zz,i}^2}}. \tag{17}$$

We could thus specify a set of N_{iso} velocity dispersions $\{\sigma_{zz,i}\}$, and fit the densities and velocity dispersions observed at each of N_z heights z_j, solving for the potential and for the density

normalizations of the individual components. However, without parameterizing the potential in some way, there are many (highly correlated) degrees of freedom in such fits: equations (16) and (17) give $2N_z$ constraints for $(N_z + N_{\rm iso} - 1)$ fit parameters (the -1 arises from the free zero point of the potential). Typically, in past applications of this method, $N_z \approx 10$ and $N_{\rm iso}$ would have to be at least three to be able to describe the data adequately. With a small number of components, it turns out (not surprisingly) that the derived potential is quite sensitive to the dispersions of the individual model components. Since we require the derivative of this potential, we really have to (and also have the freedom to) adjust the dispersions until we obtain a potential which has some expected form. This is the method used by Oort (1960) in his reanalysis of Hill's (1960) K giant data, except that because computing time was in short supply then, he calculated the fractions of the various components using a first-pass guess at the potential, rather than solving for them and the potential self-consistently. He used three isothermal components.

Rather than put no constraints on the potentials that can come out of this solution, and solve for the $\psi(z_j)$ independently, it makes more sense to use a parameterization of plausible potentials instead; this way we have many fewer parameters to play with and are guaranteed to obtain a sensible potential (if there is one that is consistent with the data), even if the choice of dispersions for the various components is not quite optimal. The resulting potential still depends on the individual $\sigma_{zz,i}$'s, though, so this method still leaves a lot to be desired.

If we need to parameterize the potentials in any case, and require at least six parameters to model the phase space density of the tracer in terms of isothermal components, there is little to be gained from not fitting a continuum of 'isothermal components'. That is the course we have taken, which is described in the following section.

3.4 CONSTRUCTING $f_z(E_z)$ FROM $\nu(\psi)$

In most K_z-studies, the density $\nu(z)$ is known to better precision than the velocity distribution. Instead of fixing the parameters of the latter, and then using these to model the density gradient, it is therefore preferable to work in the other direction, and predict the velocity distribution of a tracer in different model potentials, given its density. These velocity distribution models can then be compared with the observed velocity data.

Given a distribution function $f_z(E_z)$ and a potential $\psi(z)$, we can calculate the density $\nu(z)$, which is just a moment of f_z:

$$\nu(z) = \int_{-\infty}^{\infty} f_z(z, v_z)\, dv_z \tag{18}$$

$$= 2\int_{\psi(x)}^{\infty} \frac{f_z(E_z)}{\sqrt{2[E_z - \psi(z)]}}\, dE_z. \tag{19}$$

Reparameterizing the z-height in terms of the potential ψ, we have

$$\nu(\psi) = 2\int_{\psi}^{\infty} \frac{f_z(E_z)}{\sqrt{2(E_z - \psi)}}\, dE_z. \tag{20}$$

This equation is an Abel transform, which has the well-known inversion (see, e.g. Binney & Tremaine 1987):

$$f_z(E_z) = \frac{1}{\pi}\int_{E_z}^{\infty} \frac{-d\nu/d\psi}{\sqrt{2(\psi - E_z)}}\, d\psi, \tag{21}$$

so that there is a unique relation between $\nu(\psi)$ and $f_z(E_z)$. Because of this equivalence of $\nu(\psi)$ and $f_z(E_z)$, there is a triangular mathematical relationship between the three functions $\psi(z)$, $\nu(z)$ and $f_z(E_z)$: any one of them can be deduced from the other two. Abel inversions are somewhat unstable, but not as unstable as taking a direct derivative of the data; they are in some sense 'half-derivatives'.*

It is worth examining equation (21) in more detail, as it forms the basis of our analysis technique. It is important to note that $f_z(E_z)$ depends on the density only at points where the potential exceeds E_z, i.e. beyond the point $z = \psi^{-1}(E_z)$. Therefore, we can derive the potential at large distances from the plane from high-z data alone, without having to worry in detail about the shape of the potential nearer to the plane. Since, as we will see below, a measurement of K_z at any height relates directly to the total surface density integrated to that height, this is extremely useful, allowing us to obtain meaningful results from high-z data alone. On the other hand, because high-energy stars are present at all heights, measurements of the potential very close to the plane do require knowledge of the high-energy tail of the distribution function. Therefore either the tail of the velocity distribution at low z, or the density and potential at high z, are required to measure the potential at low z (and hence the local volume density of matter ρ_0).

When starting from a set of (z, v_z) data for the tracer population, only the first of the three quantities $\nu(z)$, $f_z(E_z)$ and $\psi(z)$ is known, as one needs the potential to be able to convert $f_z(z, v_z)$ into $f_z(E_z)$. Therefore, before being able to make an inversion such as that given in equation (21), we have to make some Ansatz about the potential, or about $f_z(E_z)$. Assuming that the tracer is isothermal ($f_z \propto e^{-E_z/\sigma_{zz}^2}$) is an example of the latter, leading to a trivial inversion to equation (13).

The essential feature of our analysis is that we avoid the assumption of isothermality, by instead postulating a range of potentials $\psi(z)$, and for each of them calculating $f_z(z, v_z)$ from $\nu(z)$. We then compare these distributions to the velocity data, and select the best-fitting model potential.

This is not a direct measurement of the potential, but rather a modelling of it, so it is important to make sure that the models are sufficiently general. On the other hand, constraints can be built into the model potentials which direct derivations from data have more difficulty coping with. For example, the analysis by Hill (1960) of a K giant sample found a $|K_z(z)|$ which started to decrease above a few hundred parsecs, which leads one to deduce negative dynamical masses – a physical absurdity. The same data were shown by Oort (1960) to be consistent with a K_z-law which did not show such a turnover. This illustrates the fact that some force laws can be ruled out on physical grounds, and so should not be included among the possible solutions (provided, of course, that acceptable fits to the data can be obtained from the restricted solution set). Consistency with the galactic rotation curve can also be built into the potentials: if we were to find a very heavy disc mass, for example, which can generate most of the local circular speed by its gravity, we would not expect also to find evidence for a massive halo in K_z.

4 From K_z to determination of the disc surface density

Given a measurement of the gravitational field $\vec{K}(R, z)$ in an axisymmetric galaxy, the total density ρ of gravitating matter follows from Poisson's equation:

$$\nabla \cdot \vec{K} = -4\pi G\rho. \tag{22}$$

*In that any Fourier component $e^{iw\psi}$ of $\nu(\psi)$ corresponds to one $\propto \omega^{1/2} e^{iwE_z}$ in $f_z(E_z)$.

In the case of a disc galaxy we can express the R-gradient in $\nabla \cdot \vec{K}$ in terms of the Oort constants of galactic rotation A and B (see, e.g. Mihalas & Binney 1981):

$$\rho = -\frac{1}{4\pi G}\left\{\frac{\partial K_z}{\partial z} + \frac{1}{R}\frac{\partial}{\partial R}(RK_R)\right\}$$

$$= -\frac{1}{4\pi G}\left\{\frac{\partial K_z}{\partial z} + 2(A^2 - B^2)\right\}. \tag{23}$$

Assuming that $(A^2 - B^2)$ varies little over the z-range of interest, the total column density $\Sigma(z)$ between heights $-z$ and z relative to the disc plane $z = 0$ is

$$\Sigma(z) = \int_{-|z|}^{|z|} \rho(z)\, dz = \frac{|K_z|}{2\pi G} - \frac{(A^2 - B^2)}{\pi G}|z|. \tag{24}$$

As disc galaxies typically have flat rotation curves far from the centre, $(A^2 - B^2) \sim 0$. There is thus a strong correspondence between the surface density to height z and the vertical force K_z. This relationship can be used in both directions, either to deduce the way the surface density varies with z (this requires very high accuracy data), or to constrain the potential above most of the disc material to be physically plausible. It is mostly with the latter possibility in mind that we investigate this correspondence in more detail, and consider the accuracy of neglecting the z-gradient of $(A^2 - B^2)$ near the disc plane.

4.1 THE ACCURACY OF K_z TO SURFACE MASS DENSITY CONVERSIONS

We will examine in turn the z-force and surface density of mass components which make up realistic mass models of the Milky Way, in order to evaluate the errors that are made when using equation (24) to derive a surface density from a measurement of K_z.

4.1.1 Double-exponential discs

The first mass component we will consider is a double-exponential disc:

$$\rho(R,z) = \rho_d e^{-R/h_R} e^{-|z|/z_0}. \tag{25}$$

The Poisson equation for such a mass distribution is solved in Appendix A in terms of Hankel transforms: there we find the potential (equation A10)

$$\psi(R,z) = -\frac{4\pi G\rho_d}{h_R}\int_0^\infty dk J_0(kR)(h_R^{-2} + k^2)^{-3/2}\frac{z_0^{-1}e^{-k|z|} - ke^{-|z|/z_0}}{z_0^{-2} - k^2}, \tag{26}$$

and the z-force (equation A12)

$$K_z(R,z) = -\frac{4\pi G\rho_d}{h_R}\int_0^\infty dk J_0(kR)(h_R^{-2} + k^2)^{-3/2} k z_0^{-1}\ \mathrm{sign}(z)\frac{e^{-k|z|} - e^{-|z|/z_0}}{z_0^{-2} - k^2}. \tag{27}$$

The surface density to height z is

$$\Sigma(z) = 2\rho_d z_0 e^{-R/h_R}(1 - e^{-|z|/z_0}). \tag{28}$$

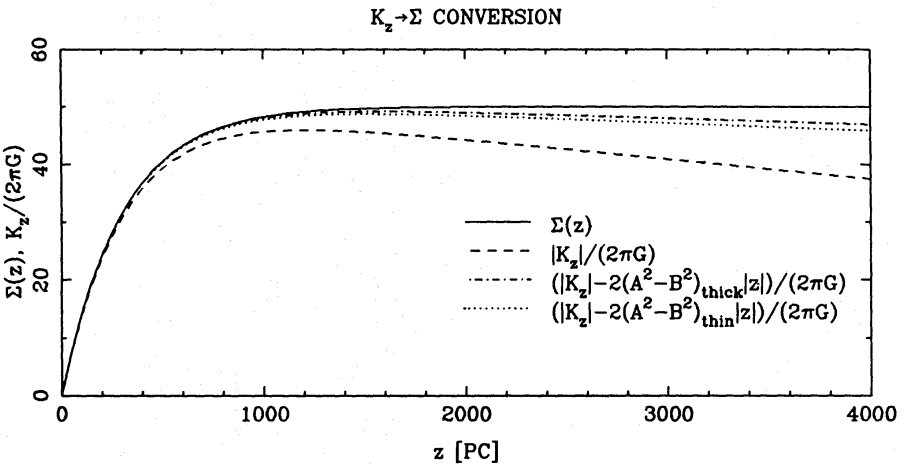

Figure 2. The surface density $\Sigma(z)$ of a double exponential disc (radial scalelength $h_R = 4.5$ kpc, vertical scaleheight $z_0 = 300$ pc) at radial distance $R = 7.8$ kpc, and approximations to it, derived from K_z and K_R. The curves are explained in the text.

Fig. 2 shows a comparison between $K_z(z)$ and $2\pi G\Sigma(z)$, for plausible solar neighbourhood parameters. While these agree quite well at low z, as expected, there is clearly a systematic, roughly linear, deviation between the two, which arises from the neglected $\partial K_R/\partial R$-term of equation (23). (Rather than write out this term in full in what follows, we continue to describe it with the Oort constants as before. Note however that these constants now refer only to the potential due to the double-exponential mass distribution above, and not to that of the entire Galaxy. To avoid confusion with the real Oort constants, when describing the potential due to a subsystem of the Galaxy, we label A and B with suffices denoting the mass component to which they refer.) On the assumption that $(A_d^2 - B_d^2)$ varies little with z, we can then calculate

$$|K_z| - 2(A_d^2 - B_d^2)_{z=0}|z|$$

as the next approximation to $2\pi G\Sigma$. This is shown as the dash-dotted line in Fig. 2, clearly a much better fit. For comparison, the dotted line shows what happens if we calculate A_d and B_d for an infinitely thin exponential disc of the same surface density as the double-exponential disc used here. The potential varies more rapidly near the plane in the thin disc case, and consequently the $(A_d^2 - B_d^2)$-term does too, yielding a slightly worse approximation to the surface density.

Rather than show a series of similar plots for different values of R, h_R and z_0, in Fig. 3 the fractional error $\Delta(\Sigma)/\Sigma$ at $z = 1$ and 2 kpc over the plausible range of values of h_R and R is plotted. Changing z_0 does not affect this significantly, as long as it remains small compared to the radial variations in ψ which cause the correction terms. The errors are clearly of the order of a few per cent. We therefore conclude that to sufficient accuracy we can approximate the z-force due to a double-exponential disc by

$$|K_z| = 2\pi G\Sigma(z) + 2(A_d^2 - B_d^2)_{z=0}|z|, \tag{29}$$

K_z taking the opposite sign to z. As will be seen later, the calculations are considerably simplified if we can express the difference $|K_z| - 2\pi G\Sigma(z)$ as a linear term in z.

4.1.2 Spherical mass components

In the case of spherical components, we do not expect such a close correspondence between $\Sigma(z)$ and $K_z(z)$, as the radial and the z-gradients of the potential are of comparable size.

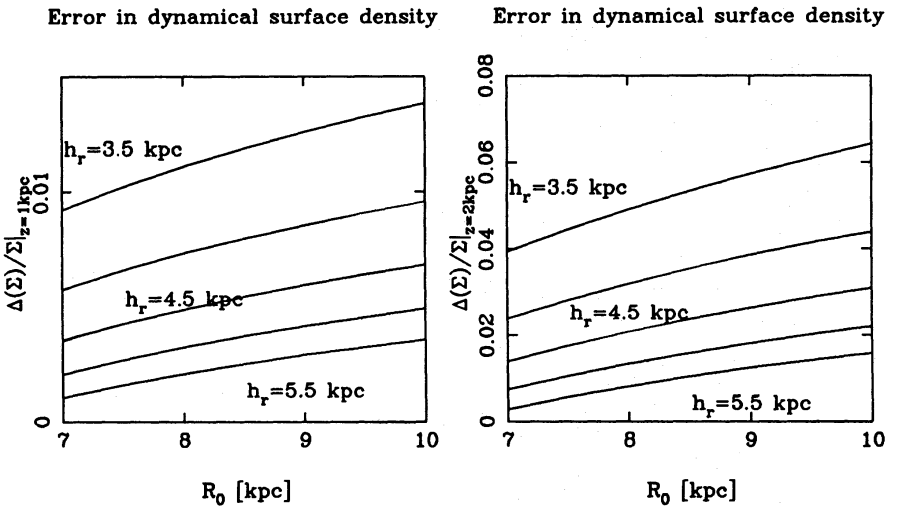

Figure 3. Fractional errors in disc surface density measurements at $z = 1$ kpc (left) and $z = 2$ kpc (right), arising from the use of equation (29). The vertical scaleheight of the disc is 300 pc.

Evaluating the correction terms is therefore of more importance for such components. If we have a mass component of density

$$\rho_s = \rho(r) \tag{30}$$

and mass profile

$$M(r) = \int_0^r 4\pi r^2 \rho(r)\, dr, \tag{31}$$

where r is the spherical radius $\sqrt{R^2+z^2}$, then

$$-K_z = \frac{GM(r)}{r^3} z \tag{32}$$

and

$$\Sigma(z) = 2\int_0^z \rho(\sqrt{R^2+z^2})\, dz. \tag{33}$$

The correction term $2(A_s^2 - B_s^2)_{z=0}$ is given by

$$\left[\frac{1}{\mathrm{R}}\frac{\partial}{\partial R}(RK_R)\right]_{z=0} = \left[\frac{1}{r}\frac{\partial}{\partial r}(rK_r)\right]_{r=R}$$

$$= \left[-\frac{1}{r}\frac{\partial}{\partial r}\frac{GM(r)}{r}\right]_{r=R}$$

$$= \frac{GM(R)}{R^3} - 4\pi G\rho(R). \tag{34}$$

Therefore, if we apply the same correction as for the disc above (see equation 29), the error we make is

$$\Delta(\Sigma)=|K_z(z)|-[2\pi G\Sigma(z)+2(A_s^2-B_s^2)_{z=0}|z|]$$

$$=\frac{GM(r)}{r^3}|z|-4\pi G\int_0^{|z|}\rho(z)\,dz-\left[\frac{GM(R)}{R^3}-4\pi G\rho(R)\right]|z| \tag{35}$$

which, expanding in z about the point $(R,z=0)$ gives

$$\frac{\Delta(\Sigma)}{\Sigma}=\frac{1}{2}\frac{z^2}{R^2}-\frac{3M(R)}{8\pi R^5\rho(R)}z^2-\frac{1}{6}\frac{d\ln\rho}{d\ln R}\frac{z^2}{R^2}+\mathrm{O}\left(\frac{z^4}{R^4}\right)$$

$$=\left[\frac{1}{2}-\frac{1}{2}\frac{\bar\rho}{\rho(R)}-\frac{1}{6}\frac{d\ln\rho}{d\ln R}\right]\left(\frac{z^2}{R^2}\right)+\mathrm{O}\left(\frac{z^4}{R^4}\right). \tag{36}$$

Here $\bar\rho$ is the average density within $r=R$. A spherical corona with a flat rotation curve has a density $\rho(r)\propto r^{-2}$, in which case $\bar\rho/\rho=3$, and the leading order correction term of equation (36) is $-\frac{2}{3}(z^2/R^2)$. In practice, we expect a corona to have some kind of core radius, which smooths down the density peak in the centre; this will decrease $\bar\rho/\rho$ and $|\Delta(\Sigma)/\Sigma|$. Thus, at $z=1$ kpc, $R=8$ kpc, the fractional error for an r^{-2} component is limited to be less than 1 per cent.

4.1.3 Composite mass models

Other mass components, either flattened or prolate, can be treated in similar ways to the above. Prolate mass distributions have smaller z-variations of K_R, so that ignoring the z-variation in A^2-B^2 is less serious than it is in the spherical case. Oblate shapes, on the other hand, are closer to the disc case, which means that the K_z-term is more important in the Poisson equation. Therefore, the spherical case is probably where we would find the most serious errors $\Delta(\Sigma)$. As we have just seen that these are perfectly acceptable for our purposes, we conclude that, for all the mass components usually considered in galactic mass models, the z-forces in the solar neighbourhood are well described by formulae of the form of equation (29).

Since the (A^2-B^2)-terms of different mass components, being proportional to K_R, add up when we build a mass model out of them, we can apply an analogue of equation (29) to the complete mass model to the same degree of accuracy. For disc galaxies, the rotation curves are usually quite flat a few disc scalelengths out from the centre (and hence $A^2-B^2\sim 0$), so that we can ignore this term completely within a few kpc from the disc plane. There is therefore a direct equivalence between $|K_z(z)|$ and $2\pi G\Sigma(z)$ over that z-range. For the Milky Way, the measured values of A and B (for a compilation see Kerr & Lynden-Bell 1986) are consistent with a flat rotation curve, after correcting for streaming motions due to the local spiral arm – see Lin, Yuan & Roberts (1978) for details. A recent measurement, of $A=11.31$ and $B=-13.91$ (both in km s^{-1} kpc^{-1}) (Hanson 1987), will need to be revised as the galactic kinematic model adopted in the analysis was inappropriate (Lewis 1989). Uncertainty in the slope of the rotation curve leaves an uncertainty of $\lesssim\pm 5\,M_\odot$ pc^{-2} in the surface density to 1 kpc, with the most probable value being zero.

The (A^2-B^2)-terms will be rediscussed below when we fit mass models to the galaxy's rotation curve.

5 Disc galaxy potentials

The method outlined in Section 3 requires a set of model potentials, out of which the best-fitting one is to be chosen. In this section, we consider plausible disc galaxy potentials, and develop a few-parameter description which includes all such potentials to a reasonable degree of approximation. It is with a grid of such potentials that we will eventually compare our dataset (Paper II).

5.1 BAHCALL POTENTIALS

For an accurate description of the z-potential near the Sun, we need to know the vertical structure of the matter distribution. This is not very well-determined. What *is* known in considerable detail, however, are the kinematics of the stars in the solar neighbourhood. Given these kinematics, it is possible to calculate the response to any given potential, and hence the vertical structure of the stellar populations observed near the Sun. By requiring that this potential be generated by the combined mass of these stellar populations, we can construct dynamically self-consistent models of the mass distribution in the solar neighbourhood. Models such as these were formulated by Bahcall (1984a), along the lines of the investigations of Woolley (1957) and Woolley & Stewart (1967). They are especially useful for studies of the total volume density ρ_0 of matter near the Sun, which rely mainly on the shape of the potential near the plane.

In this technique, the solar neighbourhood is divided into different isothermal components, each of which responds to the potential ψ *via* its velocity dispersion:

$$\rho_i = \rho_{i,0} \mathrm{e}^{-\psi/\sigma^2_{zz,i}}. \tag{37}$$

Self-consistency of the potential and the total matter density in these components then requires that Poisson's equation be satisfied, i.e.

$$4\pi G\rho = 4\pi G \sum_i \rho_{i,0} \mathrm{e}^{-\gamma/\sigma^2_{zz,i}} = \frac{d^2\psi}{dz^2}. \tag{38}$$

(here the density includes a constant 'effective halo' density, due to the halo mass and the radial gradients of the global gravitational field of the Galaxy – this term will be discussed in more detail in Section 5.2). With the boundary conditions $\psi = \psi' = 0$ at $z = 0$, this equation can easily be integrated forwards to obtain $\psi(z)$. A variety of dark matter components can be added in, using the same prescription (equation 37) as for the visible components, and the resulting potentials calculated.

A critical problem is to analyse the gas and stars into isothermal components; this can be done to reasonable precision very near the plane, but at higher z the calculated potential becomes increasingly sensitive to the precise $z = 0$ velocity dispersions and densities. The modelling of the gas is also a problem, as it accounts for about one-half of the locally identified volume density, but its precise density and spatial distribution is poorly known. Nevertheless, in the absence of detailed knowledge about the distribution of stars and gas within a few hundred pc from the plane, these models are very useful as a means of interpolating ψ over this distance range.

In Bahcall's (1984b, c) analyses of F stars and of K giants, in which he model-fitted potentials of this type, many different dark matter components were considered. Here we shall restrict ourselves to two parameters, P_{ISM} and P_{stars} – these specify the amounts of dark matter which are distributed like the observed ISM and the observed stars respectively, expressed as a fraction of the observed mass. In principle, of course, the dark matter can be distributed over

an infinite number of isothermal components, whose relative proportions can be varied almost at will. However, varying just these two parameters covers most of the plausible types of potential that one wishes to consider, and illustrates the essential features of the discussion.

5.2 A SIMPLE PARAMETERIZATION OF PLAUSIBLE K_z FUNCTIONS

As demonstrated in Section 4, $K_z(z)$ is related directly to the surface density to height z, $\Sigma(z)$. This means that the detailed distribution of the matter in the disc (whether it has a high or low scaleheight, whether its distribution is close to exponential or more like a sech^2-law,...) does not affect the high-z potential. Hence we are able to derive the disc surface density without needing to know how the mass inside it is distributed, and can investigate simpler model potentials than those required for measurements of ρ_0.

The total mass density along a slice perpendicular to the disc for a disc–halo* system is shown schematically in Fig. 4(a). At low z, the density is mostly due to the disc component, while further away from the plane the density of the halo, which at large radii is essentially constant over a few disc scaleheights, dominates. The surface density, or equivalently $|K_z|$, for such a system is shown in Fig. 4(b). This force law has the following generic features:

(i) At low z, smaller than the scaleheights of the dominant disc components, $|K_z|$ rises almost linearly, with slope $4\pi G\rho_0$.

(ii) At large z, beyond most of the mass of the disc, $|K_z|$ is again linear, but with a much reduced slope, equal to $4\pi G\rho_{\text{halo}}$.

(iii) The extrapolation of this latter linear portion back to $z=0$ has an intercept of $2\pi G\Sigma_{\text{disc}}$.

Clearly, an accurately measured K_z-profile yields the disc surface density, as well as the volume density of the halo and that of the disc at $z=0$.

We have parameterized this generic behaviour of the K_z-function in terms of a disc scaleheight D, a disc surface density K and a halo of local density F, as follows:

$$-K_z = 2\pi GK\frac{z}{\sqrt{z^2+D^2}} + 4\pi GFz, \tag{39}$$

corresponding to the potential

$$\psi(z) = 2\pi GK(\sqrt{z^2+D^2}-D) + 2\pi GFz^2, \tag{40}$$

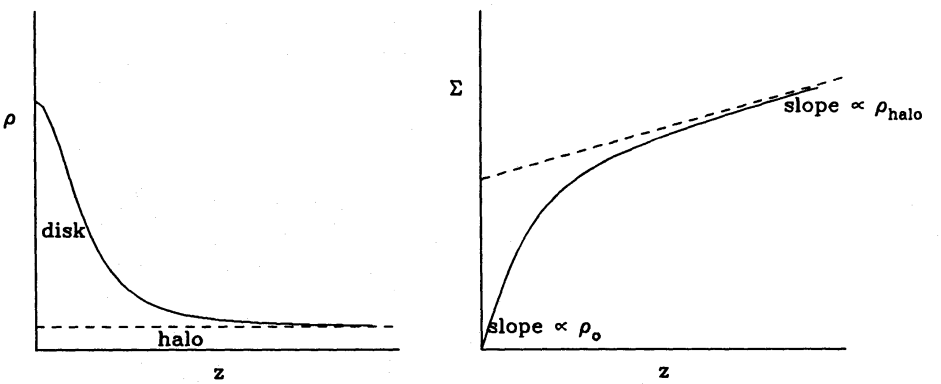

Figure 4. The volume density (left) and surface density as a function of vertical distance z from the disc plane in a simple disc–halo model.

*By 'halo' in this subsection we shall simply mean any roughly spherical mass component. Nothing is implied as regards the nature of this mass; it includes the luminous 'spheroid' or 'bulge' as well as any roughly spherical distribution of dark matter, which we shall describe by the term 'corona'.

These functions reproduce all the generic behaviour of a disc-halo system, except for the details of the disc mass distribution, which are unimportant for present purposes.

The parameter F deserves further comment. It measures the large-z quadratic term in the potential, which is predominantly caused by the halo density (taken to be constant over a few disc scaleheights). A part of it is due to the (A^2-B^2) term, however, discussed in Section 4. Because F behaves just like a constant halo density in the z-restriction of Poisson's equation, it has been termed the 'effective halo density', $\rho_{\rm eff}$. Although this name suggests that it is a function of the halo component only, this is misleading, because the quadratic part of the disc potential also contributes to the difference $\rho_{\rm halo}-\rho_{\rm eff}$.

For convenience, the quantities D, K and F will be expressed in a system of units in which distances are measured in $[L]=100$ pc, velocities in $[V]=10\,{\rm km\,s^{-1}}$, and in which $2\pi G=1$. Then there is a direct equivalence between K_z and $\Sigma(z)$, without the need for remembering the constant of proportionality. The mass scale of these units, $[M]$, is given by

$$\frac{1}{2\pi}=G=6.67\ 10^{-11}\left(\frac{\rm kg}{[M]}\right)^{-1}\left(\frac{m}{[L]}\right)\left(\frac{\rm ms^{-1}}{[V]}\right)^2, \tag{41}$$

so that

$$[M]=7.35\ 10^{35}\,{\rm kg}=367\,000\,M_\odot. \tag{42}$$

Thus surface densities come out in units of $36.7\,M_\odot\ {\rm pc}^{-2}$, and volume densities in $0.367\,M_\odot\ {\rm pc}^{-3}$, both of which are of a convenient, 'galactic', size.

5.2.1 *Consistency with the rotation curve*

As long as the rotation curve is approximately flat in the solar neighbourhood, the parameter F is dominated by the local halo density. Our strongest constraints on this density come from analysis of the galactic rotation curve, and these will have to be built into the potentials with which we are to compare our data. As the halo contributes a significant part of the potential gradient at $z\sim 1$ kpc, there is a certain amount of playoff between the disc parameter K and the halo parameter F: the lighter the disc, the heavier the halo has to be in order to make up the missing radial acceleration.

In order to translate the rotation curve constraint into a relation between K and F, we have calculated the halo parameters for a series of mass models in which the disc mass and other galactic structure parameters were varied. This is described in the next section.

6 Mass models of the Galaxy

There are two independent constraints on the gravitational potential of the Milky Way: the rotation curve of the gas, and the K_z data obtained from studies such as the present one. Combination of these two types of data can tell us a great deal about the mass distribution of the Galaxy.

Broadly speaking, the rotation curve constrains the spherical distribution of the mass $M(r)$, whereas K_z is more sensitive to the disc contribution. Together, they can thus separate the disc from the corona plus spheroid potential. Uncertainties remain, though. There is quite a strong coupling between the local corona density and the disc mass deduced from the high-z potential, due to the fact that near the solar circle the amount of corona and disc material within a kpc or so of the disc plane is similar. We will need to quantify this coupling if we are to obtain a realistic potential that is consistent with the rotation curve. For example if we find a

very heavy disc which is sufficient to explain the local circular velocity, we do not expect to find evidence for a massive corona near the solar circle, as this would push the total circular velocity beyond the local value. In fact, the disc mass is well short of being sufficient to account for the rotation curve, so the corona *is* dynamically important locally. Since we cannot accurately measure its density independent of the disc potential, though, we have to model it by fitting the rotation curve and the K_z data simultaneously. This requires that we know the shape of the dark matter corona, because the local volume density of the corona deduced from the circular velocity depends (roughly linearly) on the flattening of this component. We therefore first analyse our data (*cf.* paper II) assuming that the corona is round, and then investigate the effect of changes in the mass model and the galactic structure parameters (such as R_0, h_R, V_0). There is some evidence that dark coronae in external galaxies are indeed more round than flat, from the amount of flaring of the H I layer (Gunn 1987), and from the kinematics of polar ring galaxies (Schweitzer, Whitmore & Rubin 1983; Whitmore, McElroy & Schweizer 1987), but available constraints are very weak.

In order to consider the constraints on the corona distribution obtained from the rotation curve measurements, therefore, we have constructed a series of mass models with which to investigate the back-reaction of the disc on the coronal density.

The mass models we will investigate are those formulated by Ostriker & Caldwell (1979), and further studied in Caldwell & Ostriker (1981) (CO81) and Ostriker & Caldwell (1983). These include an exponential disc (CO81 used an infinitely flat disc, which we have here replaced with one of exponential scaleheight 300 pc), a deprojected Hubble bulge/spheroid component (henceforth the 'spheroid'), and a dark corona following Schmidt's (1985) density law. Appropriate formulae, largely taken from CO81, are given in Table 1. We have fitted these models to the gas rotation curve, obtained by combining the tangent point velocities of H I (Burton & Gordon 1978) interior to $R = 0.45\,R_0$ with the CO (carbon monoxide) data from Clemens (1985) between this radius and the solar circle. As exterior rotation curve we have used the (preliminary) results of a study of the line-of-sight motions of a sample of carbon stars at galactocentric distances of up to $2R_0$ (Schechter 1988). Results indicate that the exterior rotation curve is linear out to at least $R = 1.6\,R_0$, and yield a value of $222 \pm 17\,\mathrm{km\,s^{-1}}$ for $2AR_0$. With a local circular velocity of $220 \pm 15\,\mathrm{km\,s^{-1}}$ (Mihalas & Binney 1981), this means that the rotation curve is consistent with being flat over this range of radius. General mass models of spiral galaxies depend very sensitively on the exterior rotation curve constraint,

Table 1. The components of our mass model for the Galaxy. Formulae for the potentials of the spherical components can be found in Caldwell & Ostriker (1981), while the disc potential is derived in Appendix A of this paper.

Component	Density
Disk	$\rho = \rho_d e^{-R/h_R} e^{-\lvert z\rvert/z_0}$
Bulge/spheroid	$\rho = \rho_s \begin{cases} \frac{3.75}{Z^2}\left(\frac{3-Z}{Z^{1/2}}\left[\ln\frac{1+Z^{1/2}}{(1-Z)^{1/2}}\right]-3\right) & r<r_s \\ 1 & r=r_s \\ \frac{3.75}{Z^2}\left(\frac{3+Z}{Z^{1/2}}\left[\tan^{-1}\left(-\frac{1}{Z^{1/2}}\right)+\frac{\pi}{2}\right]-3\right) & r>r_s \end{cases}$ for $Z = \lvert(r/r_s)^2 - 1\rvert$.
Corona	$\rho = \frac{\rho_c}{1+(r/r_c)^2}$

which determines the coronal mass. Since in our models we have extra information about the disc density, the corona is already well-constrained from data to a radius of 1.6 R_0.

The input parameters for the mass models are given in Table 2, together with an estimate of their probable errors. The disc potential is completely specified in each model, with the numerical value for the fiducial model derived from the results of Paper II. The rotation curve is then fitted by allowing the corona and spheroid parameters (scalelength, solar neighbourhood density) to vary. As the spheroid scalelength does not affect the rotation curve significantly outside the inner region of the rotation curve, we have fixed it to be 80 pc, in accordance with the best-fit value of CO81. Note that the inner peak in the rotation curve, inside $R=0.1\ R_0$, is here included in the fits, in spite of suggestions that it may well be caused by non-circular motions near the Galactic Centre, perhaps associated with a small bar (Gerhard & Vietri 1986). Other model fits, in which the inner part of the rotation curve was not fitted, and the spheroid fixed to be correspondingly less massive, did not appreciably change the potential near the Sun.

Results are given in Table 3. The top line shows the final model parameters $\rho_{s,\odot}$, $\rho_{c,\odot}$ and r_c, together with the value of F and the contributions F_ρ and $F_{(A^2-B^2)}$ due to the corona + spheroid density and due to the (A^2-B^2)-term in Poisson's equation (23). This model is illustrated in Fig. 5. In order to obtain an estimate of the error in F, further models were calculated in which each input parameter in Table 2 was varied by one standard deviation, without altering the other ones. Finally, in order to evaluate the correlation between K and F in the best-fit potential, the calculations were repeated for local disc surface densities of 37 $M_\odot$ pc^{-2} and 55 $M_\odot$ pc^{-2}.

From these results, we derive the following rotation curve constraint on the parameters F and K which describe the gravitational potential in equation (39) (in our units):

$$F=0.041-0.0094\,K\pm0.008, \tag{43}$$

Table 2. The input parameters for the mass model.

	Parameter	Description
V_o	220±15kms^{-1}	Local circular speed
R_o	7.8±0.7kpc	Galactocentric distance
$2AR_o$	222±17kms^{-1}	Exterior rotation curve
$\Sigma_\odot$	46$\mathcal{M}_\odot$pc^{-2}	Fiducial disk density
h_R	4.5±1.0kpc	Disk exponential scale length

Table 3. Rotation curve fits for various choices of galactic structure parameters. The symbols are defined in the text and in Table 1.

Model	$\rho_{s,\odot}$	r_c	$\rho_{c,\odot}$	F_ρ	$F_{(A^2-B^2)}$	$F_{\rm tot}$
	$\mathcal{M}_\odot$pc^{-3}	pc	$\mathcal{M}_\odot$pc^{-3}	(10km/s)^2(100pc)$^{-2}$		
Fiducial	0.00120	2019	0.0109	0.0329	-0.0039	0.0290
V_o=205km/s	0.00119	1695	0.0077	0.0241	-0.0006	0.0235
V_o=235km/s	0.00121	2346	0.0147	0.0432	-0.0081	0.0351
R_o=7.1kpc	0.00157	1917	0.0139	0.0418	-0.0055	0.0363
R_o=8.5kpc	0.00096	2155	0.0087	0.0262	-0.0006	0.0256
$2AR_o$=205km/s	0.00121	2299	0.0119	0.0356	-0.0055	0.0301
$2AR_o$=239km/s	0.00120	1790	0.0101	0.0306	-0.0025	0.0280
$\Sigma_\odot$=37$\mathcal{M}_\odot$/pc^2	0.00120	2013	0.0118	0.0354	-0.0040	0.0314
$\Sigma_\odot$=55$\mathcal{M}_\odot$/pc^2	0.00120	2025	0.0100	0.0305	-0.0037	0.0267
h_R=3.5kpc	0.00120	2544	0.0103	0.0311	-0.0019	0.0292
h_R=5.5kpc	0.00120	1865	0.0114	0.0342	-0.0049	0.0293

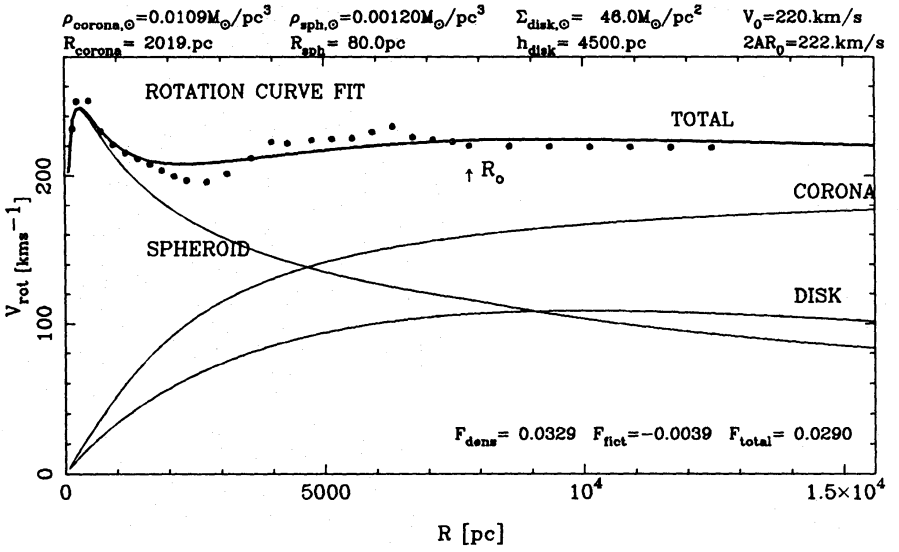

Figure 5. The rotation curve of the Galaxy, as measured from H I ($R<0.45\,R_0$), CO ($0.45\,R_0<R<R_0$) and carbon stars ($R>R_0$). The fitted model is described in the text.

which translates into

$$\rho_{\rm eff}=0.015-0.0047\left(\frac{\Sigma}{50\,M_\odot\,{\rm pc}^{-2}}\right)\pm 0.003\,M_\odot\,{\rm pc}^{-3}. \qquad (44)$$

7 Orientation of the velocity ellipsoid

So far we have assumed that E_z is an integral of the motion for our tracer population. As we saw before, it then follows that one of the principal axes of the velocity ellipsoid is aligned with the plane of the disc, and hence that $\sigma_{Rz}=0$. This considerably simplifies the dynamical analysis, as it means that we can study the z-motions in isolation, as if they made up a one-dimensional system. Unfortunately, real galaxies are more complex, and so is the mathematics required to model them.

There is no general method for constructing distribution functions which reproduce a particular density in a particular potential. Consequently we do not know exactly what the velocity ellipsoid does once the plane-parallel approximation breaks down. However, there are a few theoretical results which are useful. In Stäckel potentials (sometimes also known as Eddington potentials) analytic solutions do exist. In these potentials, the Hamilton–Jacobi equation (which yields the equations of motion in generalized coordinates) separates in confocal ellipsoidal coordinates, so that knowing the coordinate system corresponding to a particular Stäckel potential automatically yields the alignment of the velocity ellipsoid. A special case is a spherical galaxy, in which the equations separate in spherical polar coordinates, so that one axis of the velocity ellipsoid always points towards the Galactic Centre. Non-separable potentials do not have this nice property: the velocity ellipsoids of different solutions to the collisionless Boltzmann equation do not have aligned axes.

To illustrate the significance of this non-separability in determining the σ_{Rz}-term, Fig. 6 shows the projections in the (R,z)-plane of three orbits computed in the disc–halo potential described by Carlberg & Innanen (1987), using software written by R. G. Carlberg (private

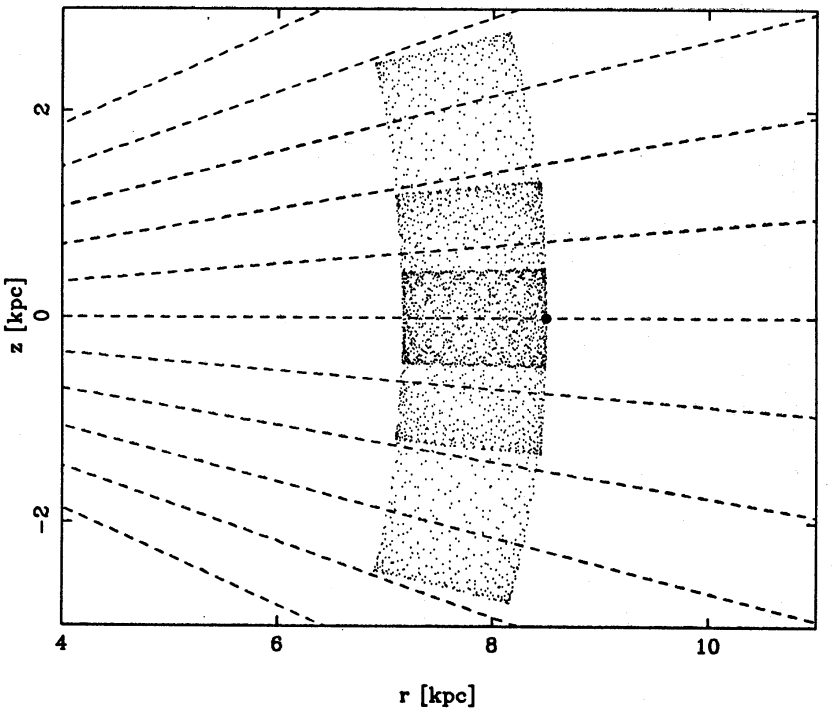

Figure 6. Three orbits in a plausible Galaxy potential. The dashed lines pass through the Galactic Centre.

communication) and J. R. Lewis (private communication). The envelopes of these orbits agree in the plane, but diverge slightly at large z. Consequently different orbits fill out boxes which are not part of a single coordinate grid, and this potential is not separable. Nonetheless, a separable distribution function can give a very good approximation to these orbits. Note that these orbits tilt towards the Galactic Centre, but not as strongly as they would in a spherical potential (in which case they would have been aligned with the dashed lines in Fig. 6). Thus one may use numerical orbit integrations to estimate the likely range of values for the σ_{Rz}-term in the Jeans' equation.

7.1 EVALUATION OF THE TILTING TERM IN THE JEANS' EQUATION

Much emphasis was placed in the previous sections on the importance of looking at the distribution function rather than just the second moment. It would be nice to be able to continue this philosophy in the case of an axisymmetric potential. To do this, we have to make a similar inversion from density plus potential to a distribution function, but now there are three integrals of motion: E, L_z and the empirical 'third integral' I_3, for which no analytic form is known. In any case, even if I_3 were known there would still be no unique solution, since ν is a function of two variables, but f of three. (This is a good reason why little is gained from using a Stäckel potential approximation in analyses of this type.) Some Ansatz about the dependence on E or L_z can be made. For example, one might specify the Toomre Q-parameter, or the rotation of the tracer stars, but then the analysis becomes more model-dependent. Rather, we will content ourselves here with two limiting cases: a uniform disc (no tilt) as described before, and a spherical potential, which might be expected if the disc contribution to the rotation curve is small. These are extreme cases, and so the effect of a spherical tilt term should be a good upper bound on the error that can be made when ignoring it (*cf.* Fig. 6 above).

We may treat the tilting term as if it is an extra force term in the Jeans' equation, and define the 'effective force'

$$K_{z,\mathrm{eff}} \equiv \frac{1}{\nu}\frac{\partial}{\partial z}(\nu\sigma_{zz}^2) = K_z - \frac{1}{R\nu}\frac{\partial}{\partial R}(R\nu\sigma_{Rz}^2) \tag{45}$$

to be the force that would be measured by an application of the 'no-tilt' Jeans' equation (10). We will model this term according to the assumptions made about the tilting of the velocity ellipsoid, and then use $K_{z,\mathrm{eff}}$ in the inversion from density to distribution function. This is not strictly accurate, as the tilting term takes a different form depending on which velocity moments one looks at; we are implicitly assuming that there is no significant change in the shape of the distribution function as a result of the tilting. Since the distribution function obtained in this way will have the correct second moment, this should be quite reasonable for present purposes.

Suppose, therefore, that the velocity ellipsoid points at the Galactic Centre. We will also assume that the axis ratio of the stellar velocity ellipsoid remains constant in spherical-polar coordinates, and has the value, in cylindrical-polar coordinates of $z=0$, $\sigma_{RR}:\sigma_{zz}=\alpha:1$. Then it is easy to show that

$$\sigma_{Rz}^2 = \frac{(\alpha^2-1)Rz}{\alpha^2 z^2 + R^2}\,\sigma_{zz}^2. \tag{46}$$

The tilting term in the Jeans' equation is $(1/R\nu)(\partial/\partial R)(R\nu\sigma_{Rz}^2)$; we therefore need the R-gradients of σ_{Rz} (and hence of σ_{zz}), and of ν. Then if the disc of the Galaxy is radially exponential, and has a constant vertical scaleheight, as is seen in external disc galaxies, vertical balance implies (for disc surface density μ) $\sigma_{zz}^2 \propto \mu$, and hence

$$\sigma_{zz}^2 \propto \mu \propto \nu \propto \mathrm{e}^{-R/h_R}. \tag{47}$$

Thus we obtain

$$\begin{aligned}\frac{1}{R\nu}\frac{\partial}{\partial R}(R\nu\sigma_{Rz}^2) &= 2(\alpha^2-1)\sigma_{zz}^2\left(\frac{\alpha^2 z^3}{(\alpha^2 z^2+R^2)^2} - \frac{Rz}{h_R(\alpha^2 z^2+R^2)}\right)\\ &\equiv T(R,z)\,\sigma_{zz}^2\end{aligned} \tag{48}$$

as the tilting term for a radially exponential population of constant vertical scaleheight with a velocity ellipsoid of constant axis ratio α which points at the Galactic Centre. $T(r_0,z)$ is graphed in Fig. 7. Note that it is negative for plausible solar neighbourhood parameters. Since this term is proportional to σ_{zz}^2, inserting it into the Jeans' equation gives a linear equation for σ_{zz}^2, from which we can deduce $K_{z,\mathrm{eff}}$:

$$\frac{\partial}{\partial z}(\nu\sigma_{zz}^2) + T(R,z)\,\nu\sigma_{zz}^2 = \nu K_z, \tag{49}$$

hence

$$\nu\sigma_{zz}^2 = -\mathrm{e}^{-S}\int_z^\infty \nu K_z \mathrm{e}^{S}\,dz, \tag{50}$$

where

$$S(R,z) = \frac{\alpha^2-1}{\alpha^2}\left[\left(1-\frac{R}{h_R}\right)\ln(\alpha^2 z^2+R^2) - \frac{R^2}{\alpha^2 z^2+R^2}\right] + \text{constant} \tag{51}$$

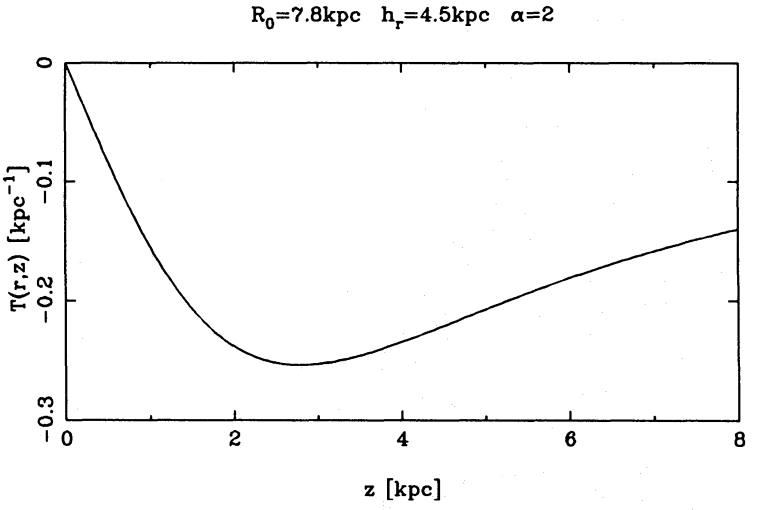

Figure 7. The function $T(R,z)$, evaluated for solar galactocentric distance 7.8 kpc, and radial disc exponential scalelength 4.5 kpc.

is the z-integral of T. Note that the effective force depends on the density law of the tracer, and will be different for different populations. Thus

$$K_{z,\mathrm{eff}} = K_z + T\frac{\mathrm{e}^{-S}}{\nu}\int_z^\infty \nu K_z \mathrm{e}^{S} dz. \tag{52}$$

We can now pretend that we still have a one-dimensional system, but with this new effective force $K_{z,\mathrm{eff}}$ instead of the true K_z, and calculate the distribution function as before. This will have the correct second moment, but the other moments will be slightly wrong – however the distribution functions are more or less isothermal at large z, so that the shape of the distribution function is quite Gaussian. The maximum likelihood fitting we use to evaluate the various models is sensitive only to the second moments for Gaussian distributions anyway, so this should not prove a serious problem. In any case the change in the shape of the distribution function will be small.

8 Comparison of models with observations: maximum likelihood

Having calculated model $f_z(z,v_z)$-distributions as described above, we have to compare them to data in order to select the best fitting one. In this work we have used maximum likelihood (Edwards 1972): this simply means that we select the model that has the highest probability

$$L(m) = \prod_{\text{data } i} \text{Prob(data point } i \text{ under model } m) \tag{53}$$

of reproducing the dataset. For continuous distributions the probability is replaced in the usual way by the probability density (as we are only interested in the relative likelihood of models, this causes no problem with normalizations). The main advantages of the maximum likelihood approach are that it does not require any binning (unlike χ^2 methods), and is non-parametric, in that it does not rely on measuring just a single dispersion parameter, but rather on fitting the entire probability distribution function.

What we observe is not in fact the phase space distribution, but the velocity distribution as a function of z, since we have not completely sampled a volume with our spectroscopic survey.

The velocity distribution at height z, $f_v(v_z;z)$, is just the conditional distribution of v_z given z,

$$f_v(v_z;z)=f_z(v_z\,|\,z)=\frac{f_z(z,v_z)}{\nu(z)}, \tag{54}$$

so the log(likelihood) of our velocity data points (z_i,v_i) for the model f_z is given by

$$\log L=\sum_i \log f_v(v_i;z_i), \tag{55}$$

which we maximize by fitting appropriate models.

8.1 THE EFFECT OF MEASUREMENT ERRORS

Errors in the data will affect the distribution of the observed stars in distance and velocity. To account for these, we convolved the models with the error distributions to obtain the distribution of *observed* position and velocity. Note that for the distance convolution we have to weight by the observing volume, since this changes with distance from the plane for an area-limited sample. Thus the distribution $F(z_{\rm obs},v_{\rm obs})$ of the observed heights and velocities in a cone of solid angle Ω towards the galactic pole is

$$F(z_{\rm obs},v_{\rm obs})=\iint \Omega z^2\,dz\,dv_z f_z(z,v_z)\,Err_z(z_{\rm obs},z)\,Err_v(v_{\rm obs},v_z), \tag{56}$$

where Err_z and Err_v are the distributions of $z_{\rm obs}$ and $v_{\rm obs}$ about the true values. The distribution of observed velocities of the stars which we observe to be at height $z_{\rm obs}$ is therefore

$$\begin{aligned}F(v_{\rm obs}\,|\,z_{\rm obs})&=\frac{F(z_{\rm obs},v_{\rm obs})}{\int dv_{\rm obs}F(z_{\rm obs},v_{\rm obs})}\\&=\frac{F(z_{\rm obs},v_{\rm obs})}{\int \Omega z^2\,dz\,Err_z(z_{\rm obs},z)\,\nu(z)}.\end{aligned} \tag{57}$$

The error distributions are approximately Gaussian in velocity and in log(distance), so

$$Err_z(z_{\rm obs},z)=\frac{1}{\sqrt{2\pi}z\sigma_{\ln z}}\,e^{-(\ln z-\ln z_{\rm obs})^2/2\sigma^2_{\ln z}} \tag{58}$$

$$Err_v(v_{\rm obs},v)=\frac{1}{\sqrt{2\pi}\sigma_v}\,e^{-(v-v_{\rm obs})^2/2\sigma_v^2}. \tag{59}$$

It is to the model distributions $F(v_{\rm obs}\,|\,z_{\rm obs})$ that the data are to be compared.

8.2 PRESENTATION OF MODEL FITTING RESULTS

The technique described in this paper predicts a range of observable distribution functions of velocity as a function of distance from the galactic plane. A separate distribution function is predicted for each adopted set of numerical values parameterizing the potential. Maximum likelihood is then used to find which of the predicted distribution functions is the best description of the observed distribution function described in Paper II.

Presentation of the quality of the maximum likelihood model as a description of the observations is somewhat problematic. Visual comparison of a contour plot of the best-fit model distribution function with contours of the observed distribution function is quite unhelpful, due to the combination of noise in the data and the complexity of interpreting the significance of any discrepancies. Similarly, plots of the relative likelihood of different combinations of numerical parameters, while useful, are difficult to relate directly to a distribution function. Hence, in Paper II, we show, in addition to such likelihood plots, a comparison of the first and second velocity moments of the model and of the observed distribution functions.

When considering these moments, it is important to consider the types of models which the maximum likelihood solution finds. If all the model distribution functions are Gaussian, the maximum likelihood value for the velocity dispersion is the rms velocity. For a distribution with more extended wings this is no longer true – e.g. for an exponential distribution, $f_v \propto \exp(-|v_z|/v_0)$, the maximum likelihood statistic is the mean modulus $|\overline{v_z}|$, which is not so strongly dominated by the wings. As the observed velocity distribution at each z distance is indeed more extended than a Gaussian, the rms is therefore not as good a statistic to use as a lower velocity moment. For illustrative purposes, to provide an estimate of the results of comparing our data with the models, we will plot the first and second velocity moments in Paper II. We emphasize, however, that the model fitting does *not* use moments of the distribution function, but fits the full distribution. The moments are plotted as a visual aid for the assistance of the reader.

9 Summary

Determination of the distribution of mass in the galactic disc near the Sun requires two complementary and almost distinct experiments. The first of these is to measure the 'Oort limit', or *volume* mass density in the plane of the Galaxy near the Sun. This experiment requires the combination of high precision local data with some supplementary distant data. A variety of determinations of the local volume mass density have been made, and are discussed further in Paper III of this series (Kuijken & Gilmore 1989b).

The second experiment is the determination of the integral *surface* mass density in a column through the galactic disc at the solar galactocentric distance. This determination requires data for distant stars, with the fundamental requirement being that one have velocity and space distribution data for a tracer population which extends above most of the total mass of the disc. The combination of both the local volume density and the integral column density of course determines (or at least severely constrains) the scaleheight of any unidentified contribution to the mass of the disc, and potentially constrains its nature. Hence the interest in these results.

In this paper we have derived a new technique for the determination of the total *surface* mass density of the galactic disc. In Paper II (Kuijken & Gilmore 1989a) we apply this technique to a new dataset to measure the integral surface mass density of the galactic disc, and in Paper III we consider the local *volume* mass density near the Sun. The essential feature of the technique described here is that one calculates the *distribution function* of velocities observed as a function of distance, for a range of plausible gravitational potentials. One then uses maximum likelihood techniques to compare the set of predicted distribution functions with the observed distribution function, so as to determine the best available description of the 'true' galactic gravitational potential.

The analysis is complicated a little by the absence of an analytic description of the full set of integrals of the motion constraining the orbits of stars in a realistic galactic potential. Thus one does not know *a priori* the orientation of the stellar velocity ellipsoids far from the galactic

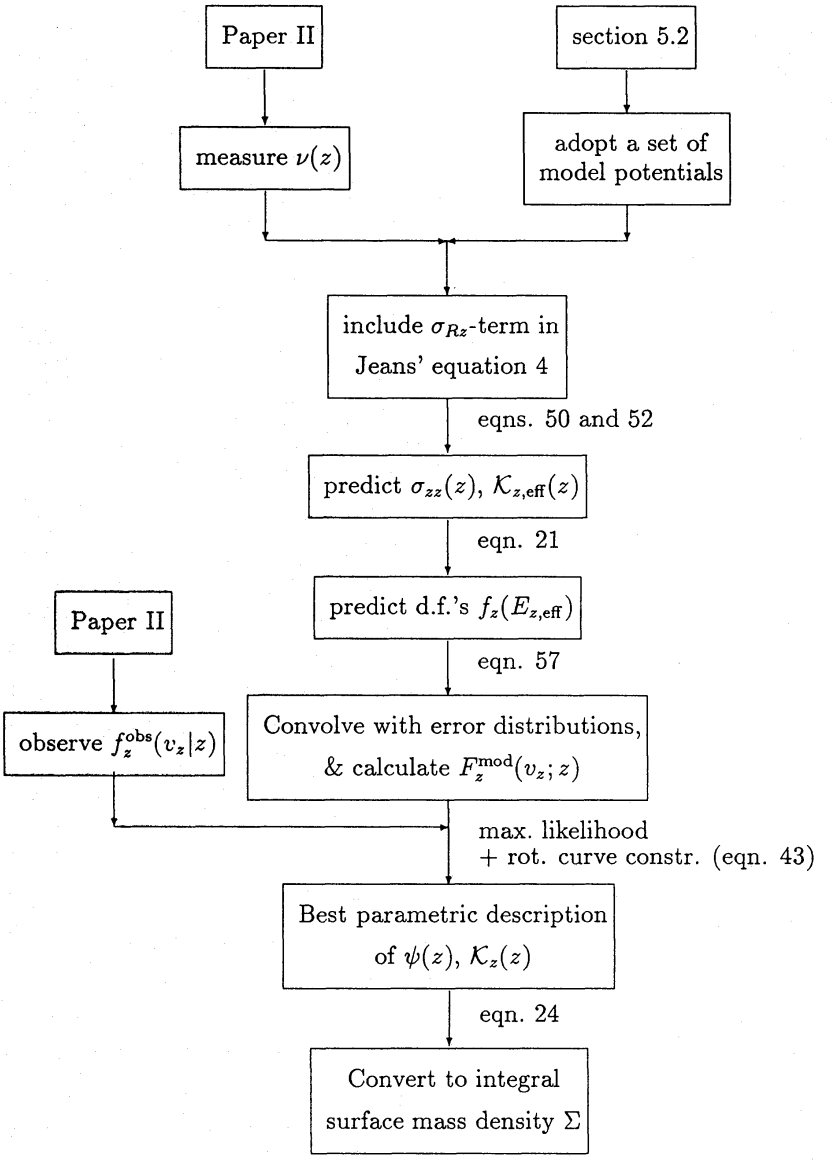

Figure 8. A summary of the technique described in this paper.

plane. This complication is handled here by considering a variety of limiting cases in the modelling procedure.

To summarize our technique, we present in Fig. 8 a flow chart, illustrating the sequence of computations used to calculate the model distribution functions. The initial calculation of the second moments is exact, while the density profile is determined by observation. Later steps in the construction of the distribution function are approximate, since $E_{z,\mathrm{eff}}$ is not an exact integral of the motion.

References

Armandroff, T. E., 1989. *Astr. J.*, **97**, 375.
Bahcall, J. N., 1984a. *Astrophys. J.*, **276**, 156.
Bahcall, J. N., 1984b. *Astrophys. J.*, **276**, 169.
Bahcall, J. N., 1984c. *Astrophys. J.*, **287**, 926.

Binney, J., 1982. In: *Morphology and Dynamics of Galaxies,* eds Martinet, L. & Mayor, M., p. 1, Geneva Observatory, Sauverny.
Binney, J. & Tremaine, S., 1987. *Galactic Dynamics,* Princeton University Press, Princeton.
Burton, W. B. & Gordon, M. A., 1978. *Astr. Astrophys.,* **63,** 7.
Caldwell, J. A. P. & Ostriker, J. P., 1981. *Astrophys. J.,* **251,** 61.
Carlberg, R. G. & Innanen, K. A., 1987. *Astr. J.,* **94,** 666.
Carney, B. W., Latham, D. W. & Laird, J. B., 1989. *Astr. J.,* **97,** 423.
Casertano, S., 1983. *Mon. Not. R. astr. Soc.,* 203, 735.
Clemens, D. P., 1985. *Astrophys. J.,* **295,** 422.
Edwards, A. W. F., 1972. *Likelihood,* Cambridge University Press.
Gerhard, O. E. & Vietri, M., 1986. *Mon. Not. R. astr. Soc.,* **223,** 377.
Gilmore, G., 1984. *Mon. Not. R. astr. Soc.,* **207,** 223.
Gilmore, G., Reid, I. N. & Hewett, P. C., 1985. *Mon. Not. R. astr. Soc.,* **213,** 257.
Gilmore, G. & Wyse, R. F. G., 1987. In: *The Galaxy,* p. 247, eds Gilmore, G. & Carswell, R., Reidel, Dordrecht.
Gradshteyn, I. S. & Ryzhik, I. M., 1980. *Table of Integrals, Series and Products,* Academic Press, London.
Gunn, J. E., 1987. *Dark Matter in the Universe, IAU Symp. No. 117,* p. 557, eds Kormendy, J. & Knapp, G. R., Reidel, Dordrecht.
Hanson, R. B., 1987. *Astr. J.,* **94,** 409.
Hénon, M. & Heiles, C., 1964. *Astr. J.,* **69,** 73.
Hill, E. R., 1960. *Bull. astr. Inst. Neth.,* **15,** 1.
Kerr, F. J. & Lynden-Bell, D., 1986. *Mon. Not. R. astr. Soc.,* **221,** 1023.
King, I. R., 1965. *Astr. J.,* **70,** 296.
Kuijken, K. & Gilmore, G., 1989a. *Mon. Not. R. astr. Soc.,* **239,** 605.
Kuijken, K. & Gilmore, G., 1989b. *Mon. Not. R. astr. Soc.,* **239,** 651.
Lewis, J. R., 1989. *Mon. Not. R. astr. Soc.,* submitted.
Lin, C. C., Yuan, C. & Roberts, W. W. Jr., 1978. *Astr. Astrophys.,* **69,** 181.
Martinet, L., 1974. *Astr. Astrophys.,* **32,** 329.
Mihalas, D. & Binney, J., 1981. *Galactic Astronomy,* Freeman, San Francisco.
Murray, C. A., 1986. *Mon. Not. R. astr. Soc.,* **223,** 649.
Miyamoto, M. & Nagai, R., 1975. *Publs astr. Soc. Japan,* **27,** 533.
Oort, J. H., 1960. *Bull. astr. Inst. Neth.,* **15,** 45.
Oort, J. H., 1965. In: *Galactic Structure,* p. 455, eds Blaauw, A. & Schmidt, M., University of Chicago Press.
Ostriker, J. P. & Caldwell, J. A. P., 1979. In: *The Large Scale Characteristics of the Galaxy,* p. 459, ed. Burton, W., Reidel, Dordrecht.
Ostriker, J. P. & Caldwell, J. A. P., 1983. In: *Kinematics, Dynamics and Structure of the Milky Way,* p. 249, ed. Shuter, W., Reidel, Dordrecht.
Sandage, A. R. & Fouts, G., 1987. *Astr. J.,* **92,** 74.
Schechter, P. L., 1988. Talk presented at CITA workshop *The Mass of the Galaxy,* 1988.
Schmidt, M., 1985. *The Milky Way Galaxy, IAU Symp. No. 106,* p. 75, eds van Woerden, H., Allen, R. J. & Burton, W. B., Reidel, Dordrecht.
Schweizer, F., Whitmore, B. & Rubin, V. C., 1983. *Astrophys. J.,* **288,** 909.
van der Kruit, P. C., 1988. *Astr. Astrophys.,* **192,** 117.
Whitmore, B., McElroy, D. & Schweizer, F., 1987. *Astrophys. J.,* **314,** 439.
Woolley, R. v. d. R., 1957. *Mon. Not. R. astr. Soc.,* **117,** 198.
Woolley R. v. d. R. & Stewart, J. M., 1967. *Mon. Not. R. astr. Soc.,* **136,** 329.
Zinn, R., 1985. *Astrophys. J.,* **293,** 424.

Appendix A: The potential due to a finite-thickness radially exponential disc

In this appendix we derive the potential due to a disc of density

$$\rho(R,z)=\rho_d e^{-\alpha R}\rho_z(z) \tag{A1}$$

for the special case

$$\rho_z(z)=e^{-\beta|z|}. \tag{A2}$$

For a general axisymmetric density $\rho(R,z)$, Poisson's equation can be solved in terms of Hankel transforms

$$\tilde{f}(k)=\int_0^\infty xdxJ_0(kx)f(x), \tag{A3}$$

where J_0 is a Bessel function, to yield the gravitational potential

$$\psi(R,z)=-2\pi G\int_0^\infty dkJ_0(kR)\int_{-\infty}^\infty d\zeta\tilde{\rho}(k,\zeta)\mathrm{e}^{-k|z-\zeta|}. \tag{A4}$$

(see, e.g. Casertano 1983). $\tilde{\rho}(k,z)$ is the Hankel transform of $\rho(R,z)$ in the R variable. If the density factorizes into a radial and a vertical part $\rho(R,z)=\rho_R(R)\rho_z(z)$, i.e. if the vertical density profile $\rho(R,z)/\rho(R,0)$ is independent of radius, this can be rearranged to

$$\psi(R,z)=-2\pi G\int_0^\infty dkJ_0(kR)\int_0^\infty uduJ_0(ku)\rho_R(u)\int_{-\infty}^\infty d\zeta\rho_z(\zeta)\mathrm{e}^{-k|z-\zeta|}. \tag{A5}$$

If the radial dependence is exponential, $\rho_R(R)=\rho_d\mathrm{e}^{-\alpha R}$, as given by equation (A1), then the u-integral can be evaluated analytically:

$$I_R(k)\equiv\int_0^\infty uduJ_0(ku)\rho_d\mathrm{e}^{-\alpha u}=-\frac{\partial}{\partial\alpha}\int_0^\infty duJ_0(ku)\rho_d\mathrm{e}^{-\alpha u}$$

$$=-\frac{\partial}{\partial\alpha}[\rho_d(\alpha^2+k^2)^{-1/2}] \tag{A6}$$

$$=\rho_d\alpha(\alpha^2+k^2)^{-3/2}, \tag{A7}$$

where equation (A6) is obtained from Gradshteyn & Ryzhik (1980) equation (6.611).

The ζ-integral of equation (A5) can be rewritten as

$$I_z(k)\equiv\int_{-\infty}^\infty d\zeta\rho_z(\zeta)\mathrm{e}^{-k|z-\zeta|}$$

$$=2\mathrm{e}^{-k|z|}\int_0^{|z|}d\zeta\cosh(k\zeta)\rho_z(\zeta)+2\cosh(kz)\int_{|z|}^\infty d\zeta\mathrm{e}^{-k\zeta}\rho_z(\zeta). \tag{A8}$$

This can again be calculated analytically if ρ_z is exponential, $\rho_z(z)=\mathrm{e}^{-\beta|z|}$ (any normalization can be absorbed into ρ_d): in that case

$$I_z(k)=2\frac{\beta\mathrm{e}^{-k|z|}-k\mathrm{e}^{-\beta|z|}}{\beta^2-k^2}. \tag{A9}$$

The apparent singularity for $\beta=k$ is not real, as can readily be verified with l'Hôpital's rule.

Thus the potential due to a double-exponential disc, of radial scalelength $1/\alpha$ and vertical

scaleheight $1/\beta$, is

$$\psi(R,z) = -4\pi G\alpha\rho_d \int_0^\infty dk J_0(kR)(\alpha^2+k^2)^{-3/2} \frac{\beta e^{-k|z|} - k e^{-\beta|z|}}{\beta^2 - k^2}. \tag{A10}$$

The radial and vertical forces, K_z and K_R, are given by the negative z- and R-derivatives, respectively. These are

$$K_R(R,z) = -4\pi G\alpha\rho_d \int_0^\infty k dk J_1(kR)(\alpha^2+k^2)^{-3/2} \frac{\beta e^{-k|z|} - k e^{-\beta|z|}}{\beta^2 - k^2}. \tag{A11}$$

and

$$K_z(R,z) = -4\pi G\alpha\rho_d \int_0^\infty dk J_0(kR)(\alpha^2+k^2)^{-3/2} k\beta \,\mathrm{sign}(z) \frac{e^{-k|z|} - e^{-\beta|z|}}{\beta^2 - k^2}. \tag{A12}$$

These integrals have oscillating integrands, so some care needs to be taken when evaluating them numerically; if this is done properly, though, the resulting convergence is quite rapid. Only for large β (small scaleheight) do we have to go to large k before the integrals converge.

If we have a different vertical density profile, for example one which is not as strongly peaked as an exponential, the I_z integral will change. In general, this will mean that a double infinite integral is required to evaluate the potential, which is very costly computationally. However, if the density profile is taken to be of the form

$$\rho_z(z) = \mathrm{sech}^\xi(\beta z/\xi) \tag{A13}$$

proposed by van der Kruit (1988), this integral, while not analytic, can nevertheless be evaluated relatively efficiently as a summed series.

If we insert the z-density (A13) into equation (A8), set $\eta = \beta/k\xi$ and make the substitution $t = e^{-k\xi}$, we obtain

$$I_z = \frac{2^\xi e^{-k|z|}}{k} \int_{e^{-k|z|}}^1 \frac{dt}{kt} \frac{t + t^{-1}}{(t^\eta + t^{-\eta})^\xi} + \frac{2^{1+\xi}\cosh(kz)}{k} \int_0^{e^{-k|z|}} \frac{dt}{t} \frac{1}{(t^\eta + t^{-\eta})^\xi}. \tag{A14}$$

As all the integrals are within the interval $[0,1]$, we can expand the terms involving $(t^\eta + t^{-\eta})^\xi$ with the binomial expansion and integrate the resulting series. This yields, after some working,

$$I_z = 2^{1+\xi} \sum_{m=0}^{\infty} \binom{-\xi}{m} \frac{\beta(1+2m/\xi)e^{-k|z|} - k e^{-(1+2m/\xi)\beta|z|}}{(1+2m/\xi)^2\beta^2 - k^2}, \tag{A15}$$

where the mth binomial coefficient of power $-\xi$ has been denoted by $\binom{-\xi}{m}$. If k, ξ and β are such that $(1+2m/\xi)\beta = k$ for some value of m, the denominator will be zero. These terms are still regular, however; to evaluate them we can use l'Hôpital's rule, as was done for the corresponding situation in equation (A9). The resulting term is then

$$\frac{2^\xi}{k} \binom{-\xi}{m} (1 + k|z|) e^{-k|z|}. \tag{A16}$$

The case $\xi = 0$ corresponds to the exponential density of equation (A2), and so should give us the same result as equation (A8). This is indeed the case: for $\xi = 0$ only the first binomial coefficient is non-zero, and this term is identical to equation (A9).

Appendix B: Regularity of orbits at the solar galactocentric radius

The results described in this paper have been obtained assuming that we are dealing with orbits which (i) obey the collisionless Boltzmann equation (i.e. have a fine-grained distribution function) and (ii) have an integral of motion akin to the energy of the vertical oscillations. We now discuss these assumptions in some more detail.

A physical fine-grained distribution function can be defined only in extreme situations. More realistically, the distribution function will quickly become more and more lumpy if examined at high resolution. In more extreme cases, some potentials allow 'chaotic' orbits, which ergodically fill a four-dimensional region of phase space (i.e. they pass arbitrarily close to each point in this region). Such orbits may possess 'strange attractors', for which it is impossible to find small volumes inside which the phase space density averaged over smaller and smaller subvolumes converges – instead, any volume element, no matter how small, through which such an orbit passes contains a continuous subvolume inside which the orbit never reaches (which would lead us to deduce a phase space density of zero for points on the orbit). In some cases, it is still possible to define an 'almost fine-grained' distribution function, in which we do not take the limit to arbitrarily small volumes; but then there is no guarantee that this function will satisfy the collisionless Boltzmann equation (Binney 1982). This problem is resolved by the interpretation of the distribution function which satisfies the collisionless Boltzmann equation as a *probability density* (*cf.* Binney & Tremaine 1987, section 4.1).

If all orbits are regular, the strong Jeans' theorem allows one to consider the distribution function as a well-behaved function of the isolating integrals of motion, so that there are no difficulties in the analysis. If there is mild stochasticity, i.e. some stars are on chaotic orbits, it is probably also acceptable to use a distribution function which is a function of the classical integrals. In this case there will typically be more than one set of approximate isolating integrals, so that one can describe a meaningful distribution function probability density, subject to additional constraints due to the need to satisfy more than one set of integrals. (We thank James Binney for emphasizing this point, and allaying our apprehensions about the possible effects of chaotic orbits.) Nevertheless, if there is more than *mild* stochasticity among the orbits of relevance in the solar neighbourhood then no analysis involving solutions of the collisionless Boltzmann equation is meaningful.

It is therefore crucial to know how important chaotic orbits are in axisymmetric potentials, like that of our Galaxy. Most of the disc stars move along roughly circular orbits, with only small excursions about an exact circle. For such orbits we can linearize the equations of motion: the gravitational accelerations are then proportional to the deviations from the circular orbit, and give rise to independent harmonic oscillations in the r- and the z-directions. This is a box orbit in the comoving meridional plane [the (R, z)-plane]. In addition to the energy and the component of the angular momentum about the axis of symmetry, these orbits respect a third integral of the motion, which approaches the energy of the z-motions in the limit of small oscillations. The radial extent of the box depends on the angular momentum: stars on orbits of higher or of lower angular momentum than that of a circular orbit of the same energy make larger excursions in the r-direction. If the azimuthal velocity of these stars is quite small compared to the local circular velocity, they will plunge deep into the inner regions of the Galaxy. As was shown by Martinet (1974), and most recently investigated by Carlberg & Innanen (1987), a mass concentration near the Galactic Centre will cause such plunging orbits

to 'lose' their third integrals. In effect, what happens is that the correlation (expressed by the third integral) between the vertical speed at apogalacticon and the maximum height which the star attains during its orbit is lost by the encounter with the galactic nucleus. This scatters the radial kinetic energy into the z-direction in a quasi-random fashion, and hence leads to great z-excursions for orbits which initially had small vertical speeds. If a significant number of the stars found near the Sun are on such chaotic orbits, then the entire basis of K_z-studies such as the one presented in this paper is flawed, as these rely on the existence of a third integral: it is precisely the relation between the maximum height reached by a star and its vertical speed at $z = 0$ that tells us the strength of the gravitational field near the disc plane.

There are many different ways in which chaotic orbits can be distinguished from regular ones. If a star moves on an orbit with three integrals, the orbit occupies a three-dimensional manifold in phase space. Specifying the position in coordinate space uses up these three degrees of freedom, and hence fixes the velocity up to finite degeneracy (fourfold in the case of box orbits, for example). This gives such orbits a very regular appearance, as the direction of motion at every point is always one of only a finite set of possibilities. If no third integral exists this is no longer true, because then the velocity vector has one real degree of freedom left. Since the spatial coordinates of a star together with the energy and the angular momentum of its orbit determine the total and azimuthal speeds, the only freedom that is left is the direction of the velocity vector in the meridional plane, which must therefore be allowed an infinite range of values. Chaotic orbits can therefore be identified by the much less regular appearance of their motion in the meridional plane. As we saw above, another manifestation of chaos is a large z-excursion in an orbit with low z-velocity at $z = 0$. Finally, the surfaces of section (see, e.g. Binney 1982) of a regular orbit are closed curves; chaotic orbits, on the other hand, ergodically fill a two-dimensional region on these surfaces.

As we have seen, the distance of closest approach to the centre of the Galaxy determines to a large extent whether a particular orbit has a third integral or not. To see how important such orbits are in the present study, we therefore need to investigate the angular momentum distribution of the stars which are found within a few kpc of the disc plane at the solar galactocentric radius. If the orbits are constrained to remain near the galactic plane, then a K_z analysis is possible.

In order to see how low the angular momentum of an orbit has to be for it to be chaotic, the potential used by Carlberg & Innanen (1987), which comprises a superposition of modified Miyamoto & Nagai (1975) 'disc-spheroids', was adapted to fit the rotation curve described in Section 6, as well as a radial exponential scalelength for the disc [given by $c. \frac{2}{3}(a^2 + b^2)^{1/2}$] and the K_z law at R_0 deduced from our K-dwarf sample. The resulting parameters are shown in Table B1. The model contains a nucleus and a more extended bulge in the centre as well as a disc, and has a rotation curve that is approximately flat to a radius of 15 kpc. The details of the outer potential are in any case of no consequence for this investigation. Orbits were calculated in this potential, using software due to R. G. Carlberg (private communication) and J. R. Lewis (private communication), for stars which cross the solar position. Fig. B1 shows the orbits in the meridional plane of a series of stars which were launched from the solar circle with vertical speeds of $40\,\mathrm{km\,s^{-1}}$, and various azimuthal speeds. As expected, stars with high angular momentum, $v_\phi > 100\,\mathrm{km\,s^{-1}}$ at the solar circle, are regular box orbits – this is not sensitive to the exact model parameters of the potential, except that if we remove the nucleus at the centre of the Galaxy (and hence ignore the peak of the rotation curve inside $r = 1$ kpc), then even orbits with zero angular momentum, which pass right through the axis of the Galaxy, are regular and remain confined to the disc plane.

Apart from the normal box orbits, we also find some tube orbits in the meridional plane, such as the orbit with initial azimuthal velocity $70\,\mathrm{km\,s^{-1}}$. These orbits arise as librations about

Table B1. The parameters of our modification to Carlberg & Innanen's (1987) fit to the galactic potential (for definitions of the symbols see their paper).

Parameter	disk-halo	nucleus	bulge
Mass ($\mathcal{M}_\odot$)	1.45 10^{11}	9.3 10^9	1.0 10^{10}
β_1	0.4		
β_2	0.5		
β_3	0.1		
h_1 (kpc)	0.325		
h_2 (kpc)	0.090		
h_3 (kpc)	0.125		
a (kpc)	2.4		
b (kpc)	5.5	0.25	1.5

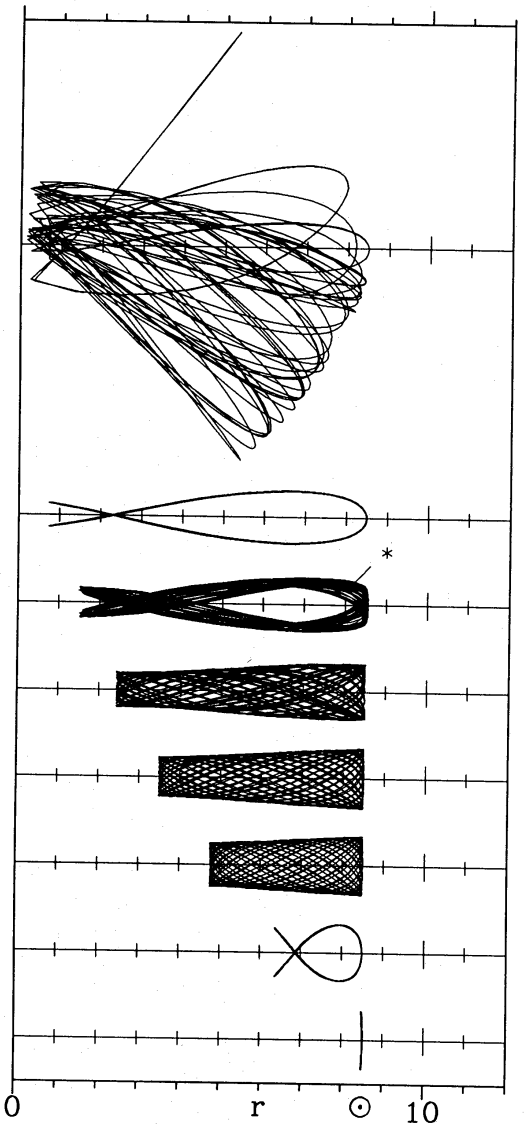

Figure B1. Meridional sections of orbits in the galactic potential described in the text. Stars were launched at the solar position with velocities $(0, v_\phi, 40)$. From top to bottom, $v_\phi = 10$, 40, 70, 100, 130, 160, 190, 220 km s^{-1}. The first orbit is chaotic, the second nearly resonant, the third a tube orbit, the following three are boxes, the penultimate one is a resonant box orbit and the final orbit is a shell orbit.

a resonant, closed orbit in the meridional plane. They are regular, but their third integrals are more complicated than those of the box orbits – nevertheless stars on tube orbits remain confined to the plane, and so can be used for a K_z study. However, if a potential allows some tube orbits, then there are usually also some, and sometimes indeed many, chaotic orbits of the same energy and angular momentum (Hénon & Heiles 1964). Hence the fact that we impose the cutoff of the angular momentum of regular orbits to be at an azimuthal velocity at the solar circle of $v_\phi = 100\,\mathrm{km\,s^{-1}}$, beyond which there are no more tube orbits. The orbit with initial azimuthal velocity $v_\phi = 190\,\mathrm{km\,s^{-1}}$, which is also resonant, does not sire any tube orbits, instead all orbits near it are normal, non-resonant box orbits.

The velocity ellipsoids of tube orbits can be strongly tilted. In some regions (e.g. near the point marked with an asterisk on the tube orbit in Fig. B1) the meridional velocities allowed to stars on such an orbit are all more or less in the same direction, unlike stars on box orbits, which cross themselves more or less symmetrically with respect to the (R,z)-coordinates. However, it seems unlikely that an observed sample of tracer stars at some point in the Galaxy would be dominated by stars with such a strong orbital tilt. Since the stellar distribution function is most likely smooth, at any point in coordinate space one would expect to see stars on box orbits, and on tube orbits with local tilts of opposite sign. The mean tilt should be much smaller than the most extreme allowed possibility.

Orbits with higher vertical crossing speeds in the plane than those shown in Fig. B1 remain regular for even lower angular momentum, since they do not approach the nucleus so closely. Thus, as long as the stars which comprise our sample of K dwarfs (Paper II) have asymmetric drifts of at most $120\,\mathrm{km\,s^{-1}}$ or so, their orbits will be almost entirely regular.

At low heights, within ~ 1 kpc of the disc plane, the stellar populations of the young and old disc dominate. These stars are well-known to have high angular momenta, with an asymmetric drift of *c.* $10\,\mathrm{km\,s^{-1}}$ (Mihalas & Binney 1981). Their radial excursions are therefore a few kpc at most, and the orbits are all boxes in the meridional plane. The classical disc population stars thus all have a well-behaved third integral.

At heights of a *c.* 1–5 kpc, the intermediate Population II (or 'thick disc') stars dominate the stellar mass. Early investigations of this population suggested that these stars, which are kinematically hotter than the old disc, had angular momenta roughly halfway between the 'classical' disc populations and those of the extreme Population II (Gilmore 1984). Such stars might thus be prime candidates for being on chaotic orbits, as unlike the stars of the extreme Population II, which have large vertical speeds which keep them from the Galactic Centre, intermediate Population II stars have relatively small vertical crossing speeds ($\sigma_{zz} \sim 40\ \mathrm{km\ s^{-1}}$ for these stars). However, the recent studies of the kinematics of nearby high-proper motion stars by Sandage & Fouts (1987) and by Carney, Latham & Laird (1989) are all in agreement over the asymmetric drift of this population, at only around $30\,\mathrm{km\,s^{-1}}$. The 'disc globular clusters' (Zinn 1985), which show a spatial and metallicity distribution similar to the thick disc stars, were thought to have a larger asymmetric drift, of $68 \pm 29\,\mathrm{km\,s^{-1}}$ – however, recent work by Armandroff (1989) shows that revised distances to some of these clusters yield a smaller value of $27\,\mathrm{km\,s^{-1}}$ for the asymmetric drift, in agreement with the local proper motion sample results. A radial velocity survey of G dwarfs *in situ* a few kpc above the plane in the direction of galactic rotation (Gilmore & Wyse 1987) also yields a high circular speed for these stars. Finally, a proper motion survey (Murray 1986) of stars up to ~ 1 kpc towards the south galactic pole yields a shear in the rotation speed of $36 \pm 5\,\mathrm{km\,s^{-1}\,kpc^{-1}}$. Thus all the observations seem to indicate that the asymmetric drift of the thick disc stars is *c.* $30\,\mathrm{km\,s^{-1}}$.

Since the azimuthal velocity dispersion $\sigma_{\phi\phi}$ of the thick disc stars is *c.* $40\,\mathrm{km\,s^{-1}}$, most of these stars will indeed have sufficient angular momentum to keep them away from trouble near the Galactic Centre. Thus it appears that the thick disc stars, like those of the thin disc, move

predominantly along regular orbits. We are therefore justified in using these stars for the present analysis.

The same is not true of the stars of the extreme population II: they have very low angular momenta on average, and a fraction of them will come very close to the galactic nucleus during their orbits, and be scattered. As shown by Carlberg & Innanen (1987), some of these stars do indeed appear to move on chaotic orbits, in that stars of very low angular momentum are statistically significantly depleted in the solar neighbourhood, as is to be expected if these stars are scattered to greater heights. However, the vertical velocity dispersion of the stars with large asymmetric drift ($v_\phi < 100\,\mathrm{km\,s^{-1}}$) is around $80\,\mathrm{km\,s^{-1}}$ in the solar neighbourhood, and hence, if such stars are present in great numbers in our sample, the velocity dispersions for the most distant stars should reflect that. As we will see in Paper II however, even our most distant stars have velocity dispersions of only *c.* $45\,\mathrm{km\,s^{-1}}$ or less. Thus extreme Population II stars are not present in our sample in significant numbers – therefore the orbits we sample are predominantly regular, validating the fundamental assumptions underlying our analysis.